Ultrastructure of the green alga *Dunaliella salina* strain CCAP19/18 (Chlorophyta) as investigated by Quick-Freeze Deep-Etch Electron Microscopy.

Jürgen E.W. Polle
1 Department of Biology, Brooklyn College of the City University of New York, Brooklyn, NY 11210, USA
2 The Graduate Center of the City University of New York, New York, NY 10016, USA

Robyn Roth
3 Center for Cellular Imaging, Washington University School of Medicine, St. Louis, MO 63110, USA

Ami Ben-Amotz
4 Marine Biology, The National Institute of Oceanography, Haifa, Israel

Ursula Goodenough
5 Department of Biology, Washington University, St. Louis, MO 63110, USA

Abstract

The single-celled green alga *Dunaliella salina* is a model system for studies on stress biology, in particular regarding secondary carotenoid accumulation. Under non-stress conditions the cells are green, but under abiotic stress the cells turn orange, because they switch their metabolism and accumulate β-Carotene in globules in the chloroplast. For the first time, Quick-freeze deep-etch electron microscopy was used to visualize cellular structures in green and orange cells of

D. salina strain CCAP19/18. This allowed us to present an in-depth analysis of the cellular ultrastructure describing and comparing the features of the two cell types. Our images illustrate the presence of a pericellular matrix for this strain of *D. salina*. The pericellular matrix was spongy and strands of unknown material anchored it into the plasma membrane. The cytoplasm contained a variety of vesicles, vacuoles, and acidocalcisomes. We could show for strain CCAP19/18 that cytoplasmic lipid bodies were often in close proximity to and sometimes in contact with the outer chloroplast envelope membrane and with the endoplasmic reticulum. Major visible differences between green and orange cells were in the chloroplast: the orange cells have greatly reduced amounts of thylakoid membranes and greatly increased numbers of β-Carotene globules. We showed that the β-Carotene globules often made point contacts with thylakoid membranes, and frequently laid side-by-side along the thylakoid membrane surface, providing support to studies that indicated exchange of molecules between β-Carotene globules and thylakoid membranes. A novel finding were the β-Carotene globule duplets, suggesting intermediate stages in β-Carotene globule morphogenesis. Overall, the β-Carotene globules appear to be similar to plant plastoglobuli. We provide this description of the cellular ultrastructure features as a resource in the context of the recent publication of the genome of *D. salina* strain CCAP19/18 to expand on the knowledge regarding this novel reference strain.

1. **Introduction**

The unicellular green alga *Dunaliella salina* TEODORESCO [1] and other *Dunaliella* species are adapted to life in hypersaline environments [2,3]. Strains of *D. salina* grow best in ~1.5 M NaCl, but they can tolerate a wide range of salinities from marine salt concentration (~0.5 M NaCl) to saturated brine solutions (~4.5M NaCl) [4,5,6].

As presented in the original description by Teodoresco [1], zoospores of *D. salina* have various shapes and forms, but are usually oval to pear-shaped and have two flagella that emerge from the anterior end of each cell. On average, mature cells are 20 µm long and 12 µm wide [1,7,8,9,10], but in some strains the cells may be > 30 µm long. Each cell contains one cup-shaped plastid with one pyrenoid, usually positioned within the lower center of the plastid. Anterior eyespots are sometimes visible by light microscopy [1,9]. Fig. 1 shows typical cells of *D. salina* strain CCAP 19/18. Under optimal, nitrogen-rich growth conditions, the cells are green in color (Fig. 1A). When cells experience abiotic stress conditions, such as nitrogen depletion and/or excess light, cells accumulate β-Carotene containing globules (βCGs) within the chloroplast and appear orange (Fig. 1B).

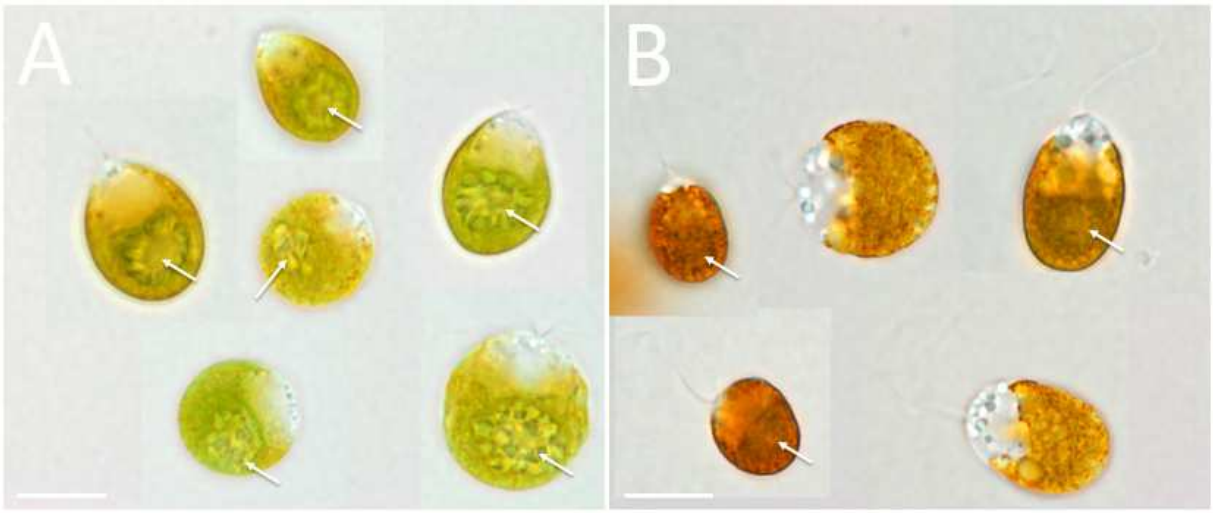

Fig. 1. Micrographs of cells of *D. salina* strain CCAP 19/18 obtained with bright-field light microscopy showing A) green non-stressed cells and B) orange cells that accumulate ß-Carotene. Arrows point out pyrenoids. A ring of starch granules surrounding the pyrenoid is more prominent in the green cells than in the organge cells. (Bars, 10µm)

Several studies have used various electron microscopy techniques to image the ultrastructure of *D. salina* or *D. bardwil* (a close relative of *D. salina* [2,10,11]). Table 1 presents a partial list of such previous publications. None of the studies used Quick-Freeze Deep-Etch Electron Microscopy (QFDEEM), an optimal technique for visualizing algal ultrastructure (12,13,14), and none interrogated the fine structure of the pericellular matrix, βCGs, and acidocalcisomes.

Table 1: Partial list of studies showing the ultrastructure of cells of the two carotenogenic species *D. salina* and *D. bardawil*. TEM, Transmission Electron Microscopy; SEM, Scanning Electron Microscopy.

Method	Study details	Reference
TEM	cross section through one orange cell of *D. salina*	15
Cryo-EM & TEM	*D. bardawil* cells from nitrogen-sufficient and nitrogen-deficient medium, supplemental movie with 3D-view through a part of an orange cell	16
Cryo-EM	green and orange cells of *D. salina* CCAP19/18	17
TEM	cross section of a green cell and an orange cell of *D. bardawil*	10
TEM	two carotene globule containing cells of *D. salina* from field samples	9
TEM	cross sections of cells of *D. salina* with focus on acidic vacuoles	18
TEM	*D. bardawil* cells green to orange, with inhibitor of carotenoid biosynthesis	19
TEM	focus on Carotene globules in *D. bardawil*	20
SEM & TEM	focus on flagella in young and mature cells of *D. salina*	21
TEM	partial cell of *D. salina* strain UTEX1644	22
TEM	various images of cells of *D. bardawil*	2
TEM	focus on polyphosphate in vacuoles in response to alkaline stress	23
TEM	cross sections of the algal chloroplast from green and orange cells of *D. bardawil*, β-Carotene and Phytoene globules.	24
SEM & TEM	SEM of one cell and TEM cross section of one βCG-containing cell of *D. bardawil*	25
TEM	orange cells and βCGs from *D. bardawil*	26
TEM	cross section of one Carotene accumulating cell of *D. bardawil*	27
TEM	cross section of one β-Carotene accumulating cell of *D. bardawil*	28
TEM & Freeze-fracture	focus on thylakoid membranes of green cells of *D. salina*	29
Freeze-etch	focus on Golgi apparatus of *D. salina*	30
TEM	general observations on ultrastructure of green cells of *D. salina*	31

For decades *D. salina* and *D. bardawil* have been model systems, mainly for studies of abiotic stress responses [32,33]. Of partiular interest were β-Carotene accumulation in stressed cells [16,26,27,32,34,35] and mechanisms of osmoregulation [2,3]. They have also been used for decades for the commercial production of β-Carotene [36,37,38]. Bioengineering efforts have included manipulating metabolism to generate production of the colorless Phytoene instead of β-Carotene [39].

Our goal in this report was to re-examine *D. salina* ultrastructure, contrasting non-stressed green cells with nutrient-stressed orange cells, and providing a general cell biology context for future systems-biology studies. We selected *D. salina* strain CCAP19/18 as a model, because the genome of this strain has recently been published [40] and functional annotations are publicly available from the US Department of Energy Joint Genome Institute either at PhycoCosm (https://phycocosm.jgi.doe.gov/Dunsal1/Dunsal1.home.html) or at Phytozome (https://phytozome.jgi.doe.gov/pz/portal.html).

2. Materials and Methods

2.1 Cultivation

D. salina strain CCAP19/18 cells were cultivated in a medium containing 1.5 M NaCl with 5mM NO_3^- [41]. Cultures were grown in batch mode in 125 mL Erlenmyer flasks kept on a platform Innova Model 2100 shaker (Eppendorf, Hauppauge, NY 11788) with 150RPM under 24-hr light provided by daylight Ecolux fluorescent lamps (General Electric Company, Boston, MA 02210, USA) at ~50 µmol photons/m^2/s. Cells in initial cultures were green, but then turned orange after about two weeks of cultivation as nutrients were depleted. Samples were taken for microscopy one week following inoculation when cells were still green and cultures were actively growing. Samples were taken again after four weeks of cultivation, when the cultures had turned orange due to the individual cells having induced carotenogenesis and stopped growth.

2.2 Light Microscopy

Aliquots of cultures were taken for light microscopy. An Olympus BX51 microscope (Olympus Corporation, Center Valley, PA 18034, USA) was used to take digital images.

2.3 Quick-freeze deep-etch electron microscopy (QFDEEM)

Pelleted live cells were placed on a cushioning material and frozen by forceful impact against a liquid-He-cooled copper block mounted within a Heuser Cryo-Press Quick-Freezing Device (Valiant Instruments, Ellisville, MO 63011, USA). Cushioning material was hard-boiled egg white that had been sliced into 1 mm slices and placed into 2% glutaraldehyde (Electron Microscopy Sciences, Hatfield, PA 19440, USA)/Phosphate Buffered Saline solution for two hours and then extensively washed with distilled H_2O. Before time of use, slices were further trimmed into smaller squares measuring 4 x4 x1 mm and then placed into physiological buffer matching the sample (1.5 M NaCl). The frozen material was transferred to liquid nitrogen and fractured under vacuum, etched at −100 ° C for 2 min and Pt/C rotary-replicated under vacuum using a Balzers BAF 400 D Freeze Etching System (Balzers AG, Lichtenstein), as described [42]. Replicas were examined with a JEOL electron microscope, model JEM 1400 (JEOL, Peabody, MA 01960), equipped with an AMT (Advanced Microscopy Techniques, Woburn, MA 01801, USA) V601 digital camera. The images are photographic negatives; hence protuberant elements of the fractured/etched surface are most heavily coated with platinum and appear white.

3. Results and Discussion

To investigate the ultrastructure of non-stressed cells, we cultivated *D. salina* strain CCAP19/18 in nutrient replete medium with 5 mM nitrate (N) in batch culture. Light microscopic images from cells of these cultures are presented in Fig. 1A. Following nutrient depletion over time, cells in the batch cultures turned orange (Fig 1B). Here, the QFDEEM technique was used to study the structural details of green and orange cells of strain CCAP19/18. All figures in the manuscript depict images of this strain.

Fig. 2 presents an overview of the basic structure of a non-stressed cell. This particular cell is oval shaped and a thin extracellular layer surrounds the cell as a pericellular matrix (lower arrow). As expected, the chloroplast is cup-shaped, oriented with the base towards the posterior side of the cell and containing one pyrenoid in the center of its base. With lobes extending towards the anterior side of the cell, the chloroplast makes up the majority of the cell. The nucleus is found towards the anterior side of the cell in the center of the cytoplasm between the lobes of the cup-shaped chloroplast. A mitochondrion, a large Golgi apparatus, a vacuole and cytoplasmic lipid bodies can also be seen in Fig. 2. The Golgi apparatus is nested between the nucleus on one side and an elongated, flattened cisterna of the endoplasmic reticulum (ER), similar to the overall structure of the Golgi in Werz and Kellner [30]. The ER surrounds almost half of the Golgi.

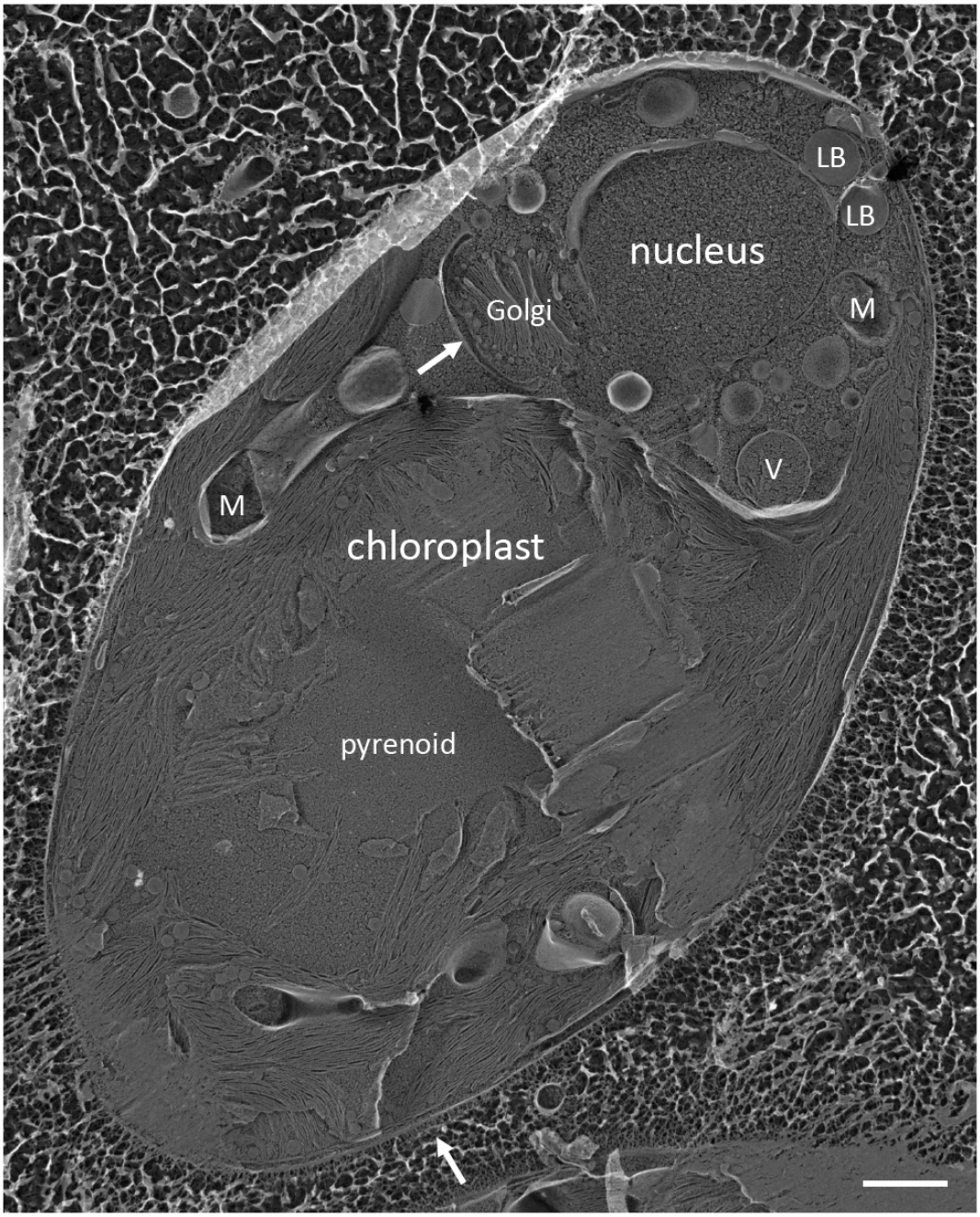

Fig. 2. QFDEEM image showing a cross-fracture through an exemplary green cell, 8 µm wide and 14 µm long. Upper arrow, ER cisternum bordering almost half of the cis side of a Golgi apparatus. Lower arrow, pericellular matrix that surrounds the cell. M, mitochondrion; LB, cytoplasmic lipid bodies; V, vacuole. (Bar, 1µm)

Fig. 3 presents additional images of cellular organization. The outer and inner membranes of the nuclear envelope, with a high density of nuclear pores, is shown in Fig. 3A. Cytoplasmic domains filled with a large number of vesicles can be seen in Figs. 3B and 3C. The cup-shape of the chloroplast is well illustrated in Fig. 3D.

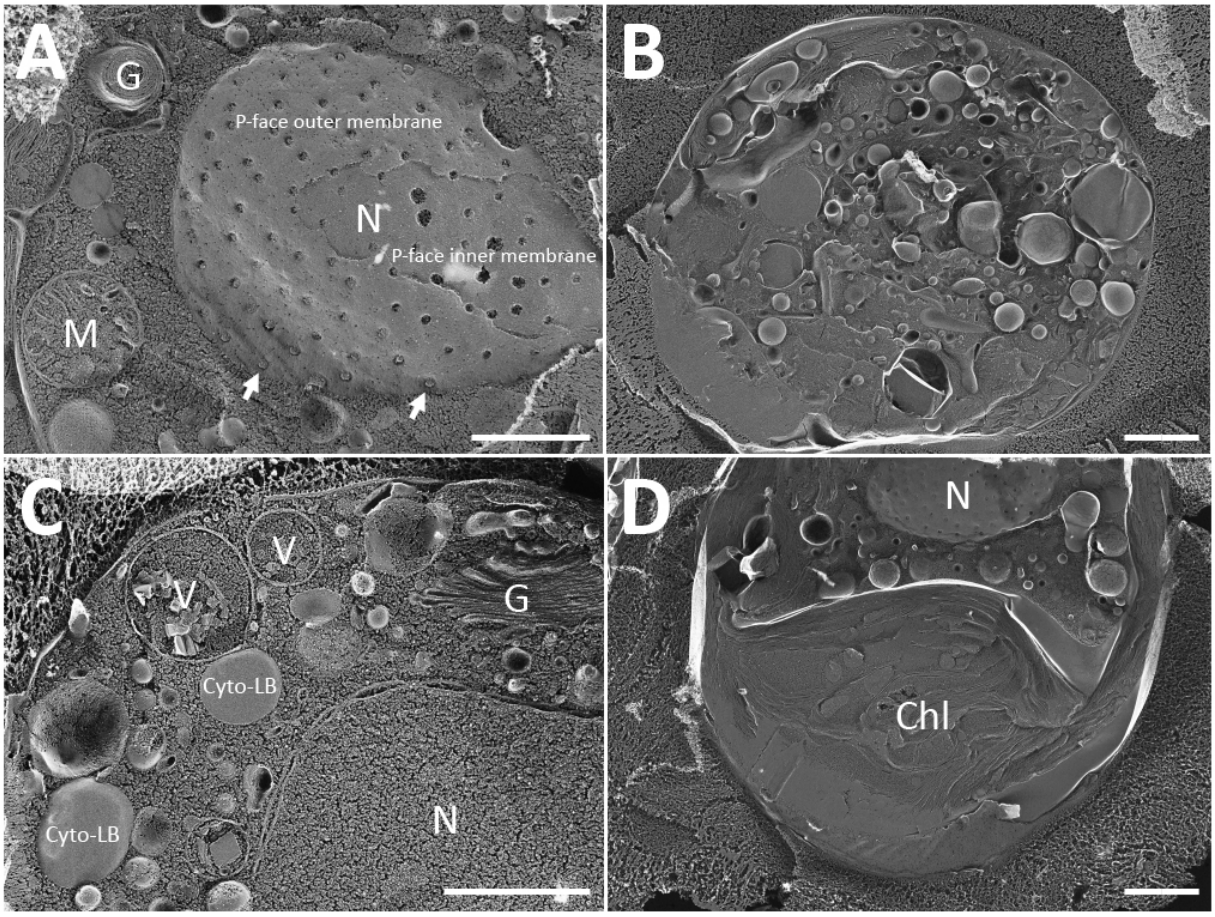

Fig. 3. A) Nuclear envelope. The fracture plane first exposes the P-face of the outer membrane and then jumps down to expose the P-face of the inner membrane. Arrows point to material that accumulates at the surface of the outer pore. B) Cross-section fracture through a cell. C) Enlarged view of the cytoplasm. D) Longitudinal fracture showing the cup-shape of the chloroplast. N, nucleus; M, mitochondrion; G, Golgi; V, vacuole; Chl, chloroplast; Cyto-LB, cytoplasmic lipid body. (Bars, 1.0µm)

3.1 Plasma membrane with pericellular matrix

A feature already recognized by Teodoresco [1] is the absence of rigid walls from cells of *D. salina*, and he noted instead a thin and smooth appearing envelope without cellulose. The presence of a pericellular matrix instead of a cell wall is believed to represent a specific adaptation to salt in *Dunaliella* species. Variation in the pericellular matrix surface pattern had also been observed in SEM for adult cells by Leonardi and Caceres [21], who described the pericellular matrix as a cell coat. To our knowledge, only some details regarding the molecular composition of the pericellular matrix are known. Sensitivity to specific enzymes suggested that the pericellular matrix of *Dunaliella* species is made up of glycoproteins and contains neuraminic acid residues [43,44]. This concept of a the pericellular matrix being a glycoprotein layer is supported by a proteomics study of the plasma membrane, which revealed the presence of bacterial type peptidoglycan-associated lipoprotein and murein lipoprotein

homologs [45]. In addition to the pericellular matrix present in zoospores, zygospores of *D. salina* also develop a cell wall, which was shown to contain sporopollenin [46]. An investigation of zygotes was beyond the scope of this study.

Using QFDEEM, we observed that the thickness of the pericellular matrix of *D. salina* strain CCAP19/18 varied from cell to cell, from being almost absent to ~ 0.5µm (Fig. 4A, 4C). The pericellular matrix appears sponge-like and is made up of numerous branched and inter-connected strands. Fig. 4 shows representative images, where the strands are mixed with globular elements in Fig. 4D. The strands are directly connected to the plasma membrane (Figs. 4B, 4C, and 4D).

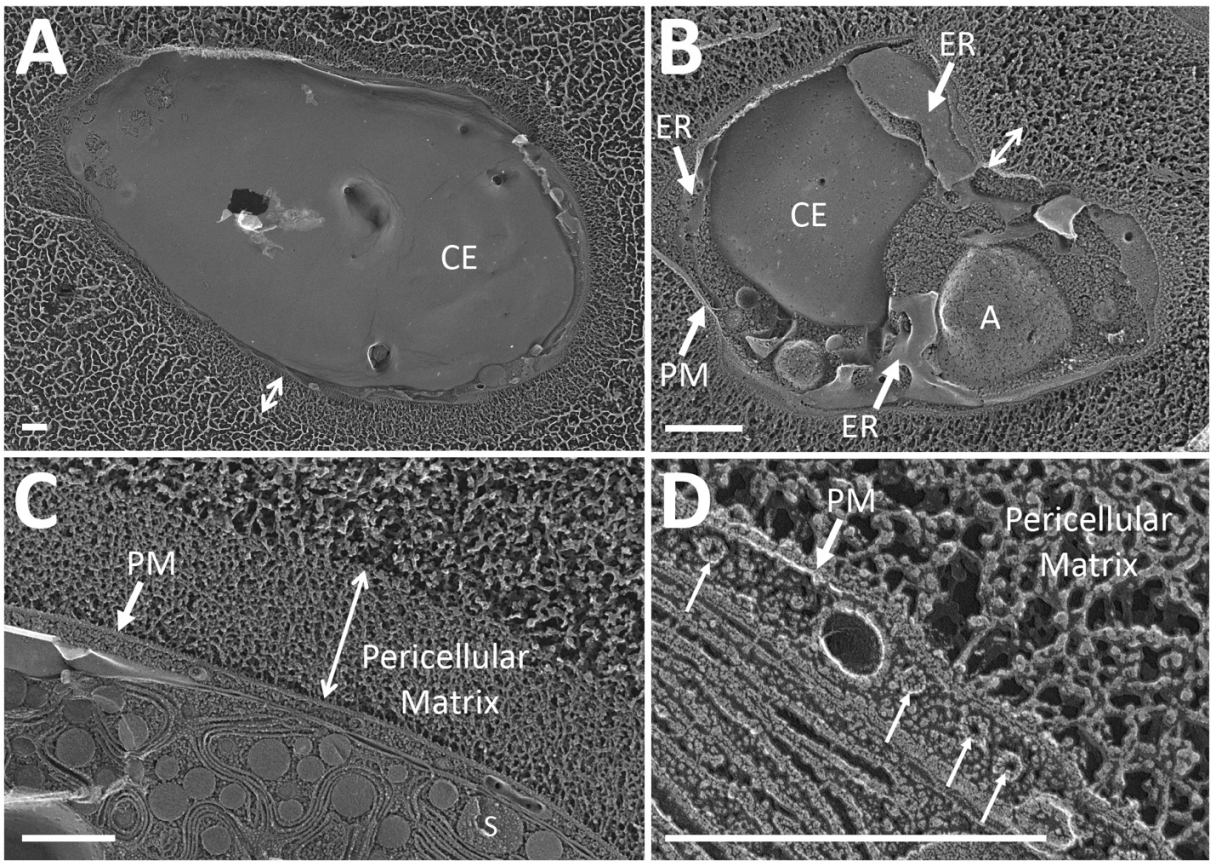

Fig. 4. A) Overview of an orange cell where the pericellular matrix is visible in cross section. The double arrow indicates its thickness. B) Top view of the pericellular matrix and the plasma membrane of a green cell surrounding the cellular interior. Fracture faces of the ER and the chloroplast envelope are indicated. C) The pericellular matrix (double arrow) from an orange cell. Carotene globules and a single starch granule are visible within the chloroplast. D) The plasma membrane and the pericellular matrix of an orange cell. The pericellular matrix is directly connected to the outer plasma membrane. Thin arrows point to microtubules that lie underneath the plasma membrane. PM, plasma membrane; ER, endoplasmic reticulum; CE, chloroplast envelope membrane; A, acidocalcisome; S, starch. (Bars, 500nm)

In the hypersaline environment that cells of *D. salina* live in, the plasma membrane is important for maintaining homeostasis, including ion and glycerol balance, assuring that

intracellular glycerol accumulation balances the high salinity outside of the cell [2,47,48]. The plasma membrane was shown to include sterol peroxides as major constituents that may be an adaptation to hypersaline conditions [49]. It is implicated in sensing changes in ions and salinity [2,50], and plasma membrane-localized carbonic anhydrases play a role in carbon acquisition under high salt conditions [51]. More recently, studies of the proteome revealed changes in the protein composition of the plasma membrane proteins as part of the acclimation responses to different salinities [45].

3.2 Nucleus

Cells have round or oval nuclei filling a large part of the cytoplasmic space (Figs. 2, 3, and 5). Figs. 5A and 5B show fractures where the two nuclear envelope membranes can be distinguished. A nucleolus is visible in Fig. 5A. Figs. 3A, 5C and 5D show fractures through the interiors of the envelope membranes: the inner membrane is displayed in Fig. 5C, and both membranes are displayed in Figs. 3A and 5D. The pores, ~ 75nm in diameter, are usually filled with material representing the nuclear pore complex.

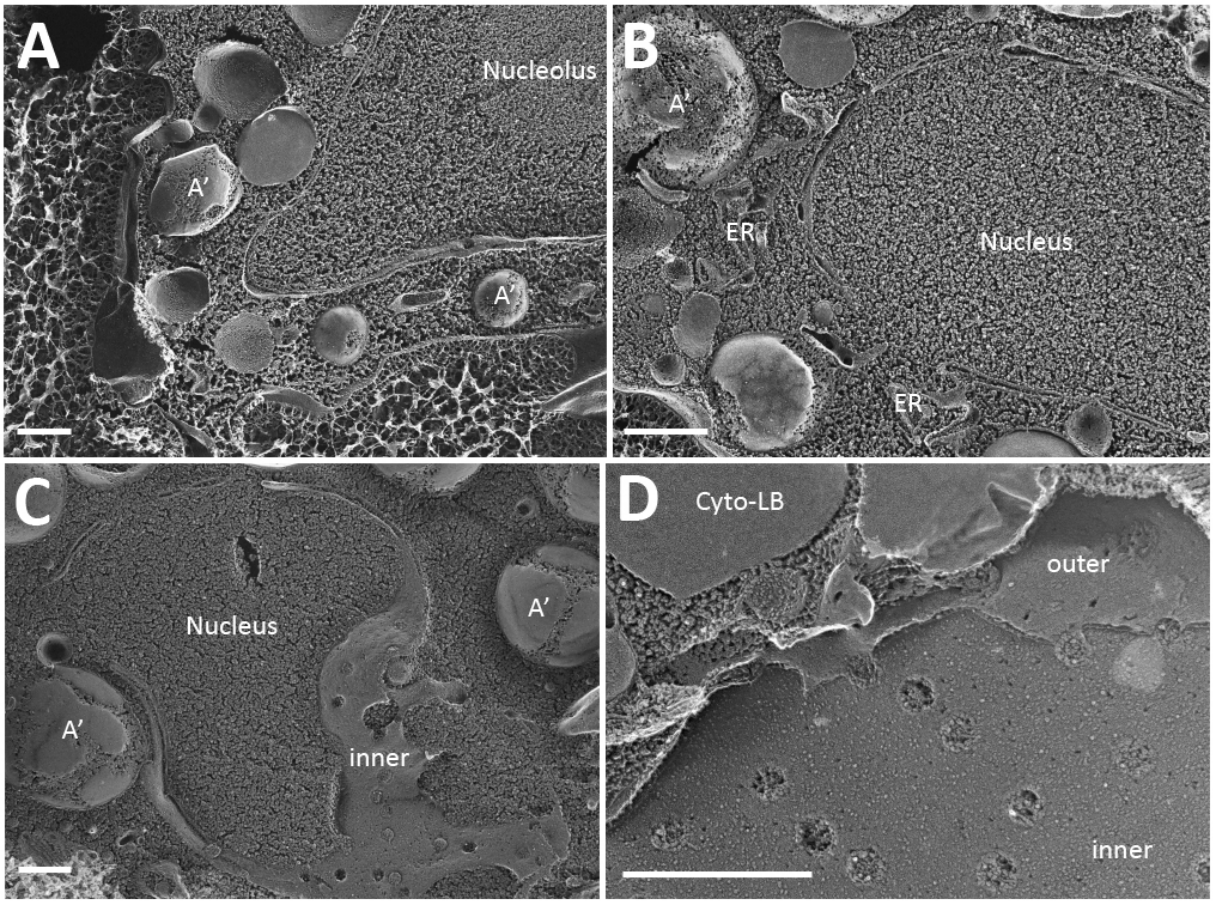

Fig. 5. Nucleus. A) Cross fracture showing nucleolus. B) Cross fracture with ER in proximity to the nuclear membrane. C) The fracture face of the inner nuclear membrane can be seen in the lower right side of the image. D) Nuclear pores visible from the cytoplasm orientation (lower right). The outer envelope is

partially visible and then the fracture extends down to the inner envelope. A', acidocalcisome variant; Cyto-LB, cytoplasmic lipid body; ER, endoplasmic reticulum. (Bars, 500nm)

3.3 Cytoskeleton

Microtubules provide most of the cytoskeletal infrastructure in flagellated green algae [21,52]. They typically underlie the plasma membrane and also associate with the flagellar apparatus. Fig. 4D shows microtubule cross-fractures beneath the plasma membrane, where their protofilament substructure can be resolved; Fig. 6 shows cross-fractures in the region of the flagellum, and includes a fibrous element associated with the flagellar apparatus. The sheets of the fibrous element are about 100nm thick and almost 1µm long.

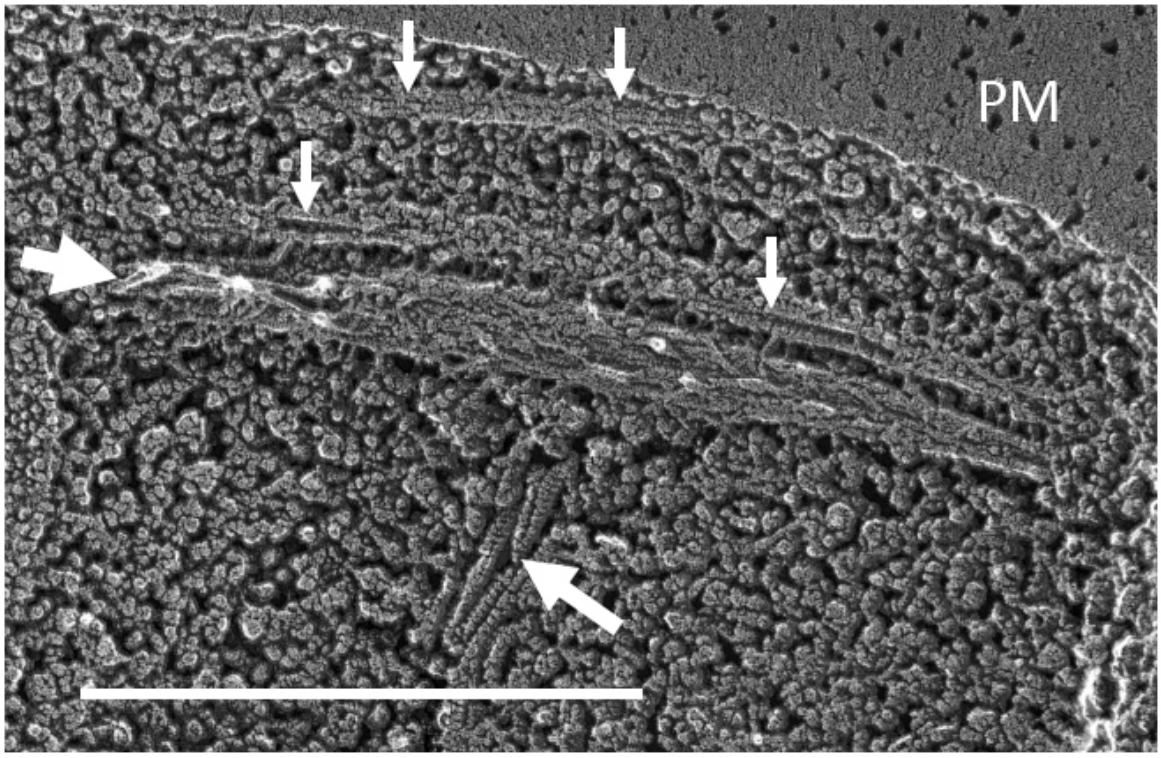

Fig. 6. Elements of the cytoskeleton. Longitudinal fractures of microtubules at small arrows. The large arrow on the left points to a fibrous root associated with the flagellar apparatus. The longer arrow at the bottom points to a domain of unidentified filamentous material, possibly derived from microtubules. PM, protoplasmic fracture face of the plasma membrane. (Bar, 500nm)

3.4 Flagella

Zoospores of *D. salina* have pairs of flagella that are at least as long as the main body of the cells. Since Leonardi and Cáceres [21] reviewed in detail the flagellar structure of *D. salina*, it is not our focus here, except to show an image of the flagellar membrane fracture face in Fig. 7A and a tangential cross section of a flagellum in Fig. 7B.

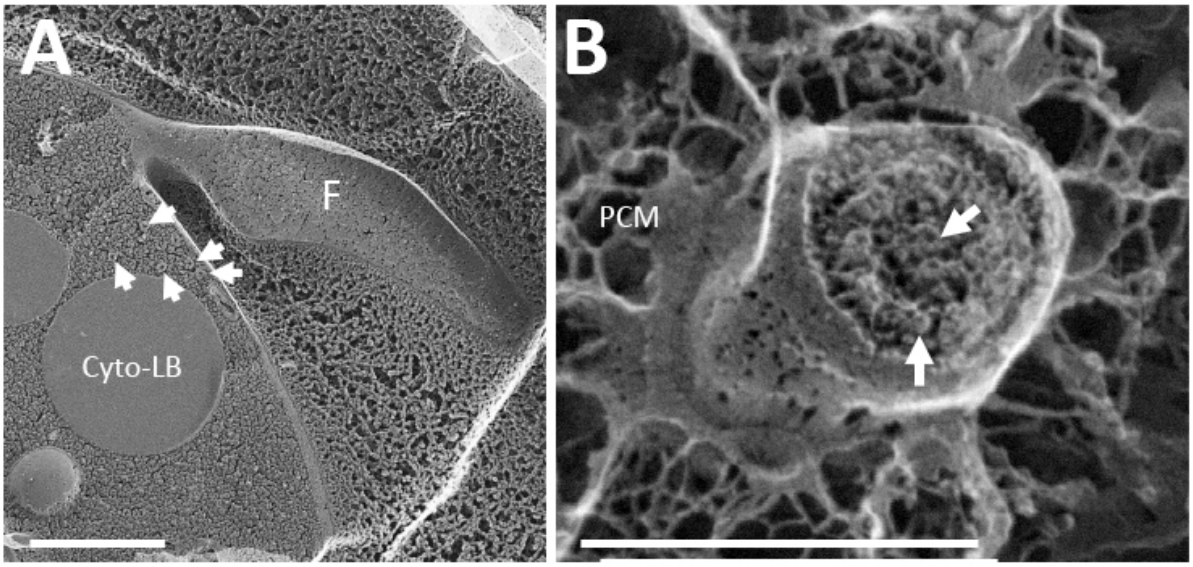

Fig. 7. Flagella in two orientations. A) A flagellum at the anterior end of a green cell showing the continuity of its membrane with the plasma membrane. Arrows: cross-fractures of microtubules. B) Cross-fracture through a flagellum of a green cell with the axoneme including the outer ring of microtubule doublets (arrow pointing upwards) and the inner central pair of microtubules (arrow pointing downwards) being visible. F, flagellum; Cyto-LB, cytoplasmic lipid body; PCM, pericellular matrix. (Bars, 500nm)

3.5 Chloroplast and Mitochondrion

Green and orange cells contain either one or multiple mitochondria, where Z-stacked images are needed to distinguish between these alternatives. Mitochondrial cross-fractures have a width of 0.5 to 1.0µm, and profiles are often sausage-shaped, as previous noted by Trezzi et al. [31]. Mitochondria occasionally extend into the lobes of the chloroplast (Fig. 8), creating intimate proximity between the two organelles.

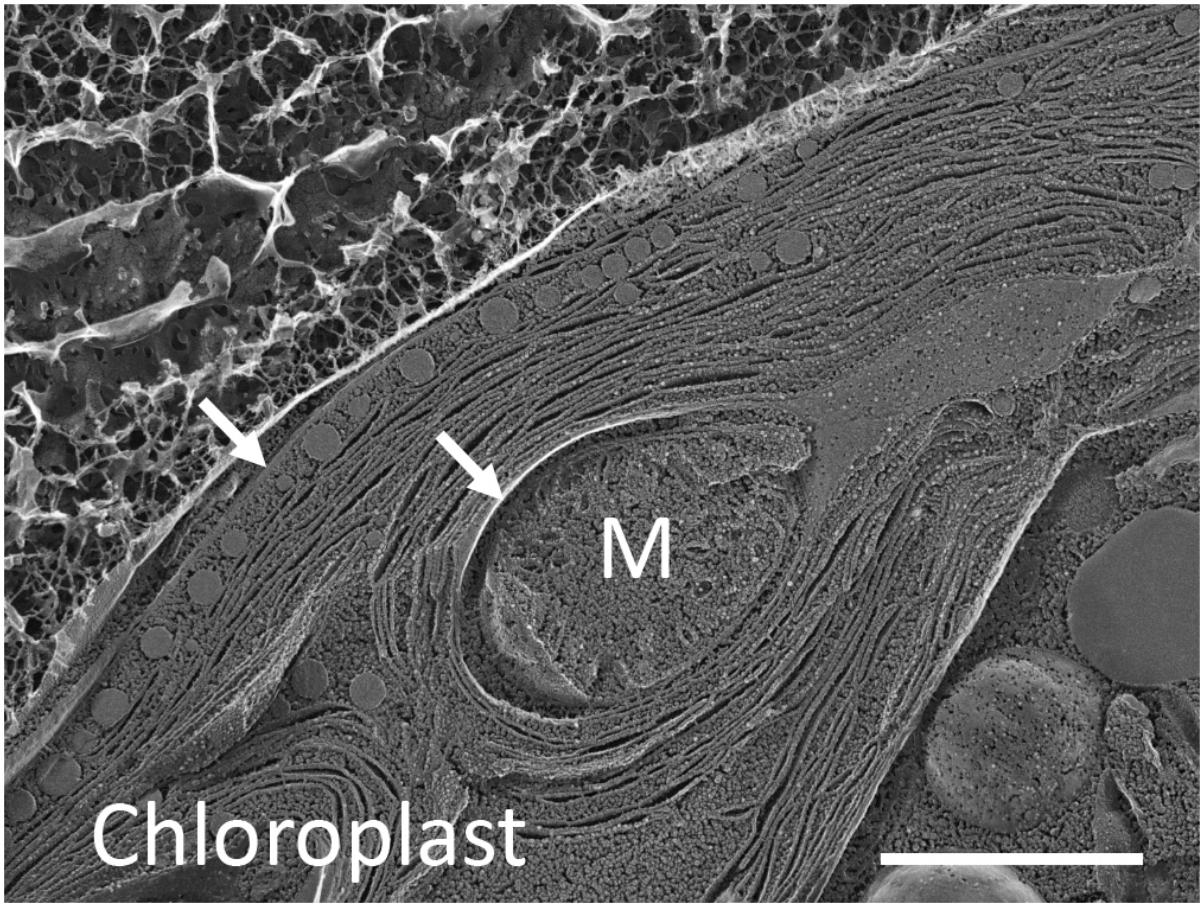

Fig. 8. Mitochondrion (M) within a lobe of the chloroplast of a green cell. Arrows point to the chloroplast envelope. (Bar, 1µm)

3.5.1 Thylakoids

Most of the thylakoids in chloroplasts of green cells are arranged in parallel stacks (Fig. 9A) [17,29]. A clear division between grana and stroma thylakoids is not evident, in contrast to land plants, as is also the case for the unicellular green flagellate and close relative *C. reinhardtii* [53]. As already noted by Pfeifhofer and Belton [29], thylakoids run mostly parallel to the chloroplast envelope (Fig. 8, Fig. 9A).

In stressed cells of *D. salina* and *D. bardawil*, chlorophyll levels are reduced to 50% or less compared with green cells [17,39], while β-Carotene levels increase more than 10-fold [27,54]. This dramatic change in pigment content is accompanied by a complementary reduction of the amount of thylakoid membrane and the appearance of large numbers of βCGs in the chloroplast (Fig. 9A versus 9B), an accumulation that colors the chloroplast orange-brown (Fig. 1). This transition, observed in both *D. salina* and *D. bardawil*, is reminiscent of the chloroplast-to-chromoplast conversion found in land plants [55].

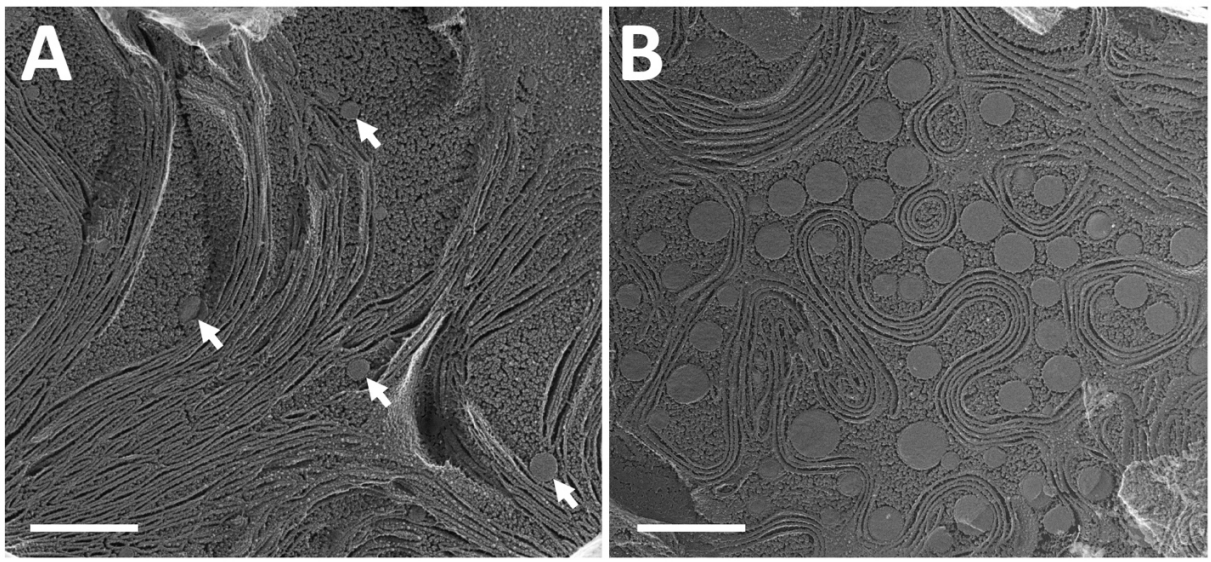

Fig. 9. Plastids. A) Green cell where the thylakoid membranes are largely arranged in parallel oriented stacks. Single β-Carotene globules at arrows. B) Orange cell where stacking of the thylakoid membrane is much reduced and the thylakoids meander through a stroma filled with β-Carotene globules. (Bars, 500nm)

The thylakoids are also dramatically reorganized: instead of the large stacks found in green cells (Figs. 8 and 9A), the thylakoids align, but make only occasional contact, meandering through the stroma and sometimes forming concentric rings (Fig. 9B).

3.5.2 Starch and Pyrenoid

Starch grains were found throughout the plastid stroma in both green and orange cells (Fig. 10). In green cells, the pyrenoid can be surrounded by a heavy starch endowment (Fig. 1A) or it can have little (Fig. 2) or moderate (Fig. 11) associated starch, a variability also encountered in *Chlamydomonas*. The pyrenoid matrix of green cells carries tubular elements derived from thylakoids (Fig. 2, Fig. 11). Unlike *Chlamydomonas* and most algae [56], however, and as previously noted for other strains of *D. salina* [15] and *D. bardawil* [24,10], these tubules never reach the center or pass through the entire pyrenoid matrix.

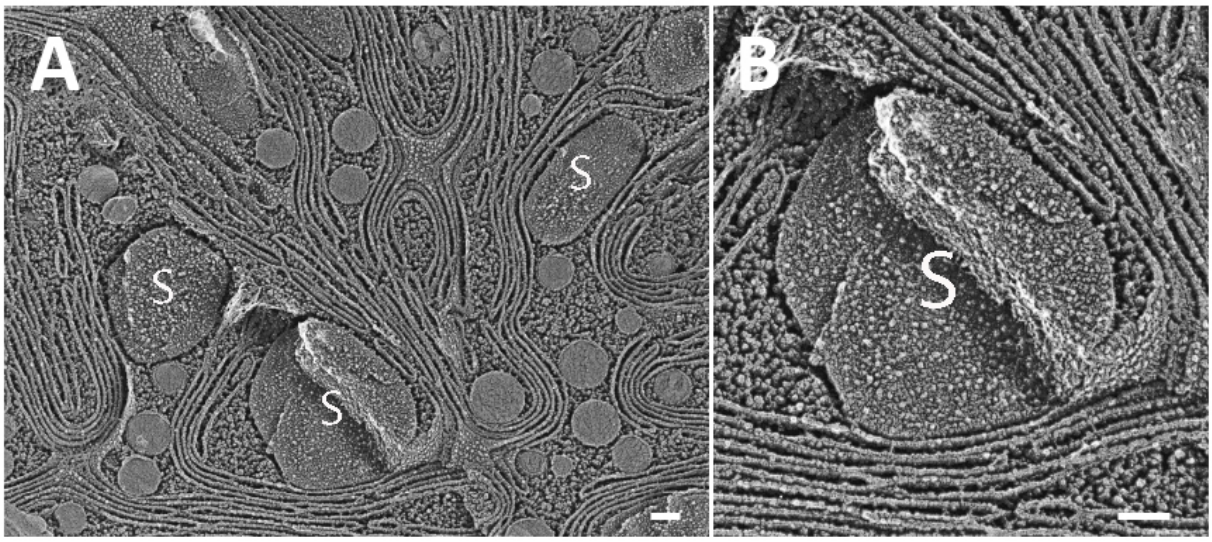

Fig. 10. A) Starch granules in the plastid of an orange cell. B) Enlarged view of one of the starch grains in (A) showing the close proximity of thylakoid membrane to the starch granule. S, starch granule. (Bar, 100nm)

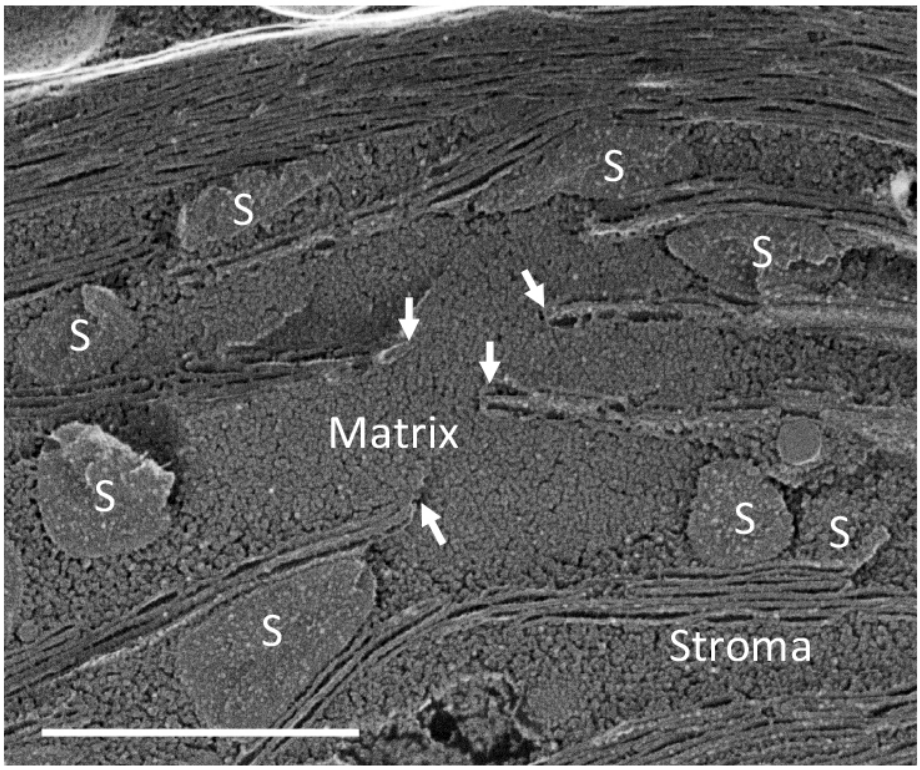

Fig. 11. Enlarged section of the green cell from Fig. 3D showing the pyrenoid with tubules entering the interior of the matrix in between starch granules. Tips of the tubules are indicated by arrows. S, starch granule. (Bar, 1µm)

In orange cells of *D. salina* [15] and *D. bardawil* [10], the central pyrenoid has been shown to be similarly organized to green cells. In the strain CCAP19/18, some orange cells have a clearly visible pyrenoid (Fig. 1, arrows), but a pyrenoid was not discernable in cells that contain large amounts of βCGs, and Davidi et al. [16] reported a complete disintegration of the pyrenoid in orange cells of *D. bardawil*. We encountered no pyrenoid images in our QFDEEM samples of orange cells.

3.5.3 Beta-Carotene Globules (βCGs)

Most flagellated green algae construct eyespots (= stigmas) (for a review see [57] and references therein) that contain βCGs. In green *D. salina* cells, the βCGs are located in an eyespot region that is often not observable by light microscopy (Fig. 1). When the eyespot is observed, it is typically diffuse [9], in contrast to the punctate domain found in *D. viridis* and *D. tertiolecta* [7,9,58] and in the closely related *C. reinhardtii* [59]. The eyespot is used as a characteristic for species identification within the *Dunaliella* genus (reviewed in [8] and [9]).

D. salina is known to be phototactic [60], indicating that it can sense the direction of light even though the eyespot may not be as well structured as in other green flagellates. Also, a gene coding for a channel rhodopsin had been identified previously in the genome of *D. salina* strain CCAP19/18 and had been compared to that of other organisms [61].

In QFDEEM images, we identified candidate eyespots for green cells of *D. salina* strain CCAP19/18 as a single row of loosely affiliated globules (Figs. 8 and 12), similar to the eyespot structures shown in TEM images of Trezzi et al. [31] and Borowitzka et al. [37], packed between the thylakoid membrane and the inner chloroplast envelope membrane. This irregular structure of the eyespot in *D. salina* probably explains why it is described as diffuse and cannot be discerned easily by light microscopy. Since orange cells accumulate βCGs throughout the chloroplast, no eyespots are discernible in orange cells.

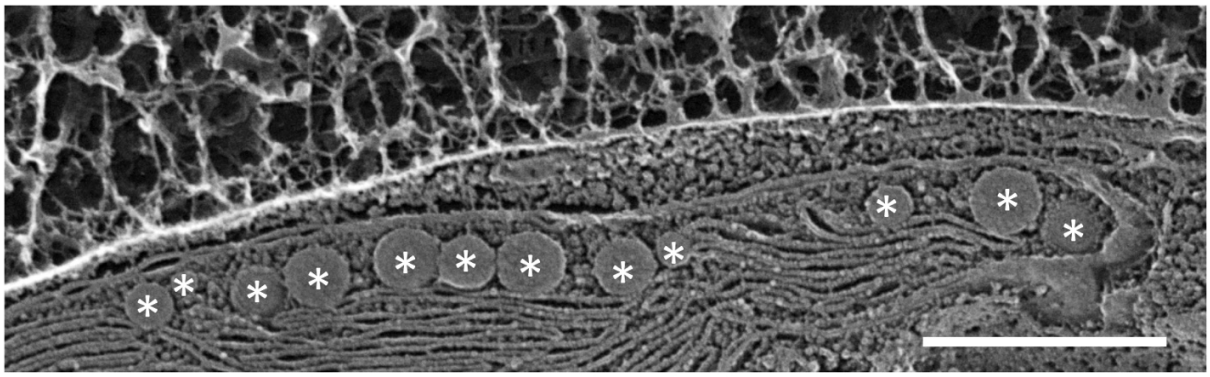

Fig. 12. Shown is an enlarged part of the cell presented in Fig. 2, here focusing on the cross section of a candidate eyespot. The candidate eyespot globules, indicated by asterisks, lie in between the chloroplast envelope and stacks of thylakoid membrane. (Bar, 500nm)

In addition to the putative eyespot globules, chloroplasts of green cells of strain CCAP19/18 have additional βCGs scattered throughout the stroma (Fig. 9A arrows) that look identical to those in the candidate eyespots, with a maximal cross section of less than 175nm. They are also

indistinguishable from the chloroplast inclusions found in *C. reinhardtii*, and designated as plastoglobules, which have a maximal diameter of 150nm [59]. Little is known about the relationship between the eyespot and the dispersed ßCGs, although it has recently been postulated [35] that βCGs evolved from the eyespot globules in *D. salina.*

When cells of *D. salina* or *D. bardawil* become stressed, for example by nutrient deprivation or exposure to high light, cells accumulate βCGs (Figs. 9B and 10A). The strong enrichment of βCGs makes stressed cells appear orange when observed by light microscopy (Fig. 1), which imparts an orange color to water bodies when *D. salina* blooms. The βCGs in orange cells are larger (maximal width of 250nm) than those in green cells, but otherwise look identical.

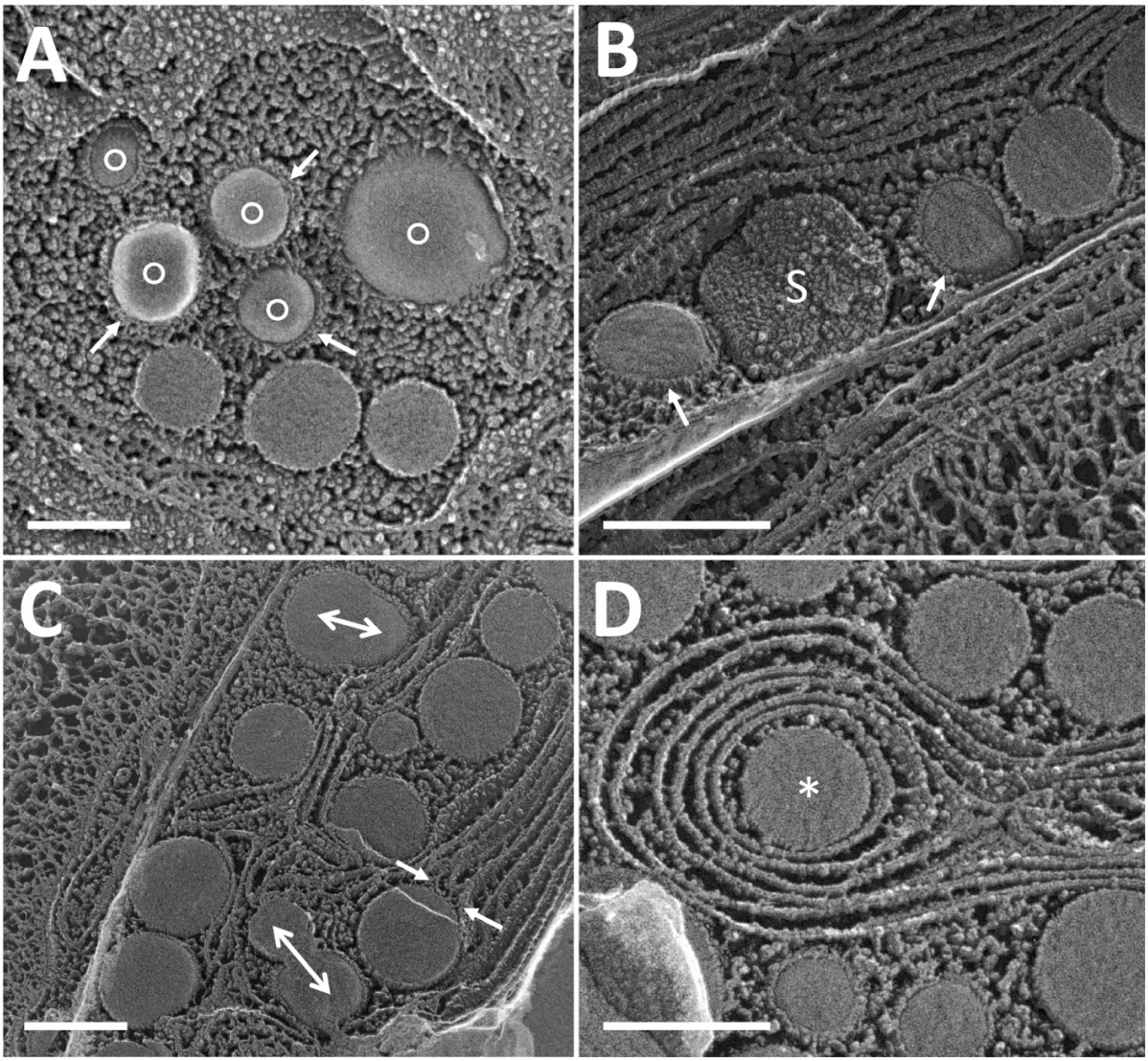

Fig. 13. Overview of β-Carotene globules (βCGs) in chloroplasts of orange cells. A) Some βCGs in top view are labeled with round circles. Thin arrows point to the coats surrounding βCGs that are exposed by etching when the fracture plane passes through the apices of the globules. B) Tangential cross-fractures through some βCGs and a starch granule (S). Two βCGs where coats are visible are pointed out

by arrows. C) Cross-fractures of βCGs. Two carotene globules appear to be duplets (double arrows). βCGs are often in punctate contact with thylakoid membrane segments (single arrows). D) Thylakoids arranged in a concentric ring around a cross-fractured βCG labeled with an asterisk. (Bars, 200nm)

Many βCGs in strain CCAP19/18 are surrounded by visible material that we refer to as a coat (Figs. 13A and 13B, arrows), which in *D. bardawil* contains a 38-kD CGP protein [20]. Thylakoid membranes frequently make punctate contacts with ßCGs, either at the thylakoid tips (Fig. 13C) or along their surfaces. Similar contacts were described for plastoglobules in *C. reinhardtii* [59]. In orange cells, βCGs can be surrounded by concentric rings of thylakoid membrane (Fig. 13D). This close contact may indicate that βCGs engage in an exchange of molecules with thylakoid membranes, a hypothesis that is also supported by results from a lipid study in *D. bardawil* showing that the lipid composition of βCGs is similar to that of chloroplast membranes [16].

The accumulation of βCGs in response to stress is dependent on triacylglycerol biosynthesis [19], and it had been suggested that β-Carotene is made within the βCGs [62]. In this context, the protein composition of βCGs has recently been analyzed from *D. bardawil* [62] revealing 116 core proteins including the unique CGP protein [16,20] and several plastid lipid-associated proteins (PAPs) in the fibrillin family; these proteins are likely included in the coats visible in QFDEEM images. Enzymes participating in carotenoid metabolism as well as in secondary metabolism were also found [62].

All told, the βCG proteome is similar to that of plastoglobules of higher plants [62], and the βCGs from *D. salina* strain CCAP19/18 look like plant plastoglobules ([63] and our images). Therefore, we propose that the βCGs are plastoglobules specialized for β-Carotene accumulation, similar to plastoglobules found in plant chromoplasts [64].

In land plants, plastoglobules have been reported to nucleate from thylakoid membranes [65,66]. It is not evident from our QFDEEM images that this is the case in *D. salina*. As noted above, many βCGs made point contacts with thylakoid membranes (Figs. 13B, 13C, 13D), but they still appear to be distinct from the thylakoid membrane, and the lipid interiors show no sign of merging. Since some βCGs appear as duplets (Figure 13C, double arrows), they may bud off each other, meaning nucleation of new βCGs from preexisting βCGs [65]. Also, we would like to mention the hypothesis that βCGs are formed from cytoplasmic lipid bodies (Cyto-LBs) [16].

3.6 Endoplasmic Reticulum (ER) and Cytoplasmic Lipid Bodies

The endoplasmic reticulum in *D. salina* takes the form of flattened cisternae or tubules, originating from the outer nuclear envelope membrane and extending into the cytoplasm (Fig. 14). ER membranes are in proximity to the Golgi cisternae (Fig. 2), vacuoles, oil bodies, and acidocalcisomes. Often the ER membrane is directly pressed against the membranes of the other cellular organelles.

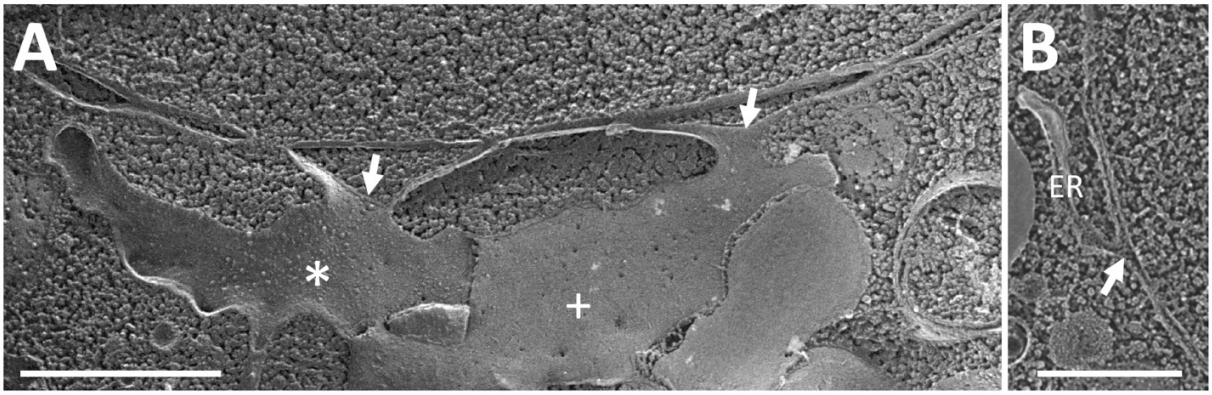

Fig. 14. Endoplasmic reticulum (ER) association with the outer nuclear envelope membrane in orange cells. A) Protoplasmic-fracture face (*) and exoplasmic-fracture face (+) of the ER membrane. B) Direct connection between the envelope and ER. (Bar, 500nm)

Triacylglycerol (TAG) metabolism and its regulation in microalgae has been intensely studied in the past decade and major progress has been made in our understanding of its molecular basis [67,68]. The protein and lipid compositions of Cyto-LBs for *D. bardawil* have been published [69,16,62,19]. In *D. bardawil* the cellular levels of glycerolipids increased by large amounts due to accumulation of new TAGs when cells were nitrogen limited [16]. In contrast, for *D. salina* strain CCAP19/18, it had been shown that the overall glycerolipid content was not dramatically different between green and orange cells, but the fatty acid profiles were dissimilar when cells were light-stressed [17] or nitrogen-stressed [70,71]. Under nitrogen-stress it had been shown that a reduction in polar lipids was accompanied by simultaneous increases in TAGs [71].

Lamers et al. [17] include images of Cyto-LBs in a Cryo-EM study of green cells of strain CCAP19/18. QFDEEM has been used to visualize the Cyto-LBs that accumulate under nitrogen-stress conditions in the related alga *C. reinhardtii* [59]. The Cyto-LBs shown here for green (Figs. 2, 3, 7, 8, 15) and orange (Fig. 16D) cells were indistinguishable from those of *C. reinhardtii*. They vary in size, with a diameter of up to 1µm, and are found throughout the cytoplasm, often nested against the outer chloroplast envelope membrane and/or next to the ER membrane (Fig. 15B), as is the case with *C. reinhardtii* [59]. When in close proximity to or directly touching one another, they retain their individuality (Fig. 15A). In contrast to many other microalgae [72] including *C. reinhardtii* [59,73], *D. salina* strain CCAP19/18 did not shown stress-induced glycerolipid accumulation in response to N-depletion [70], and we observed no increase in Cyto-LB profiles in orange vs. green cells.

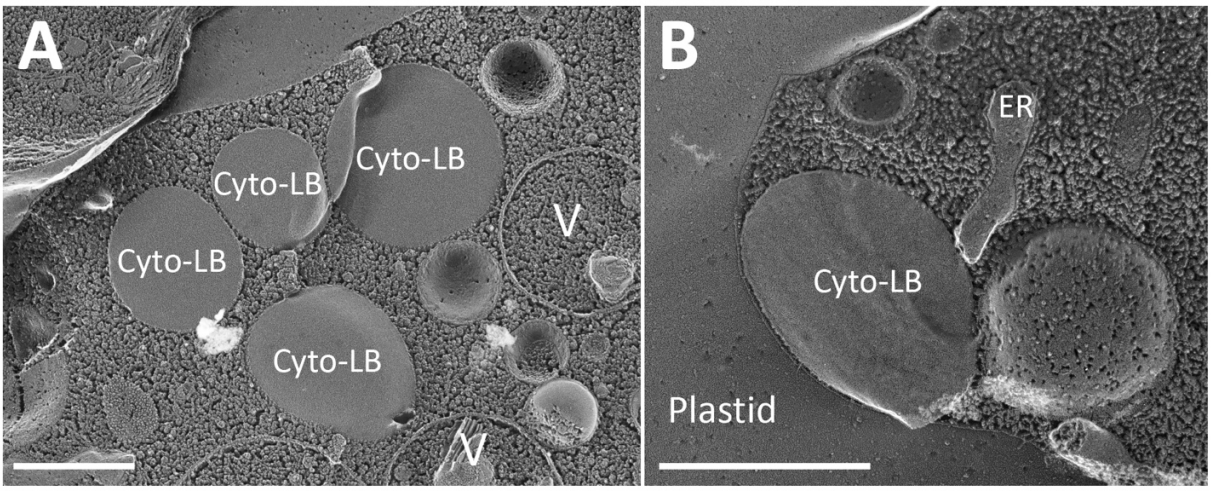

Fig. 15. Cytoplasmic lipid bodies (Cyto-LB). A) A group of lipid bodies from a green cell. B) A green cell wherein a lipid body is in direct contact with both the outer membrane of the chloroplast envelope and the endoplasmic reticulum (ER). (Bars, 500nm)

3.7 Golgi Apparatus

In eukaryotic cells the Golgi system is essential to vesicular transport of materials, and in plant and algal cells, the Golgi plays a major role in the synthesis of cell wall material [74]. In land plants, the Golgi consists of stacks of flattened cisternae from which small vesicles bud off [75]. Although *D. salina* does not have a traditional cell wall, its pericellular matrix may be made up of glycoproteins [43], and glycoproteins acquire their sugar residues in Golgi cisternae.

Previous studies had shown that multiple Golgi bodies are present in each *D. salina* cell [21], most having >10 cisternae per stack [30]. We have confirmed these observations using QFDEEM (Figure 16A and 16B). The Golgi stacks, 500nm to 1µm in cross-fracture, display a polar structure with cis- and trans-faces (Figures 16B and 16C) and a trans-Golgi network (Fig. 16B). Vesicles are observed between ER cisterna and the cis-face of the Golgi (Fig. 16B). As illustrated in Figure 16C, the Golgi cisternae may curve to generate an overall dome-shaped structure with the outermost layer being an ER membrane.

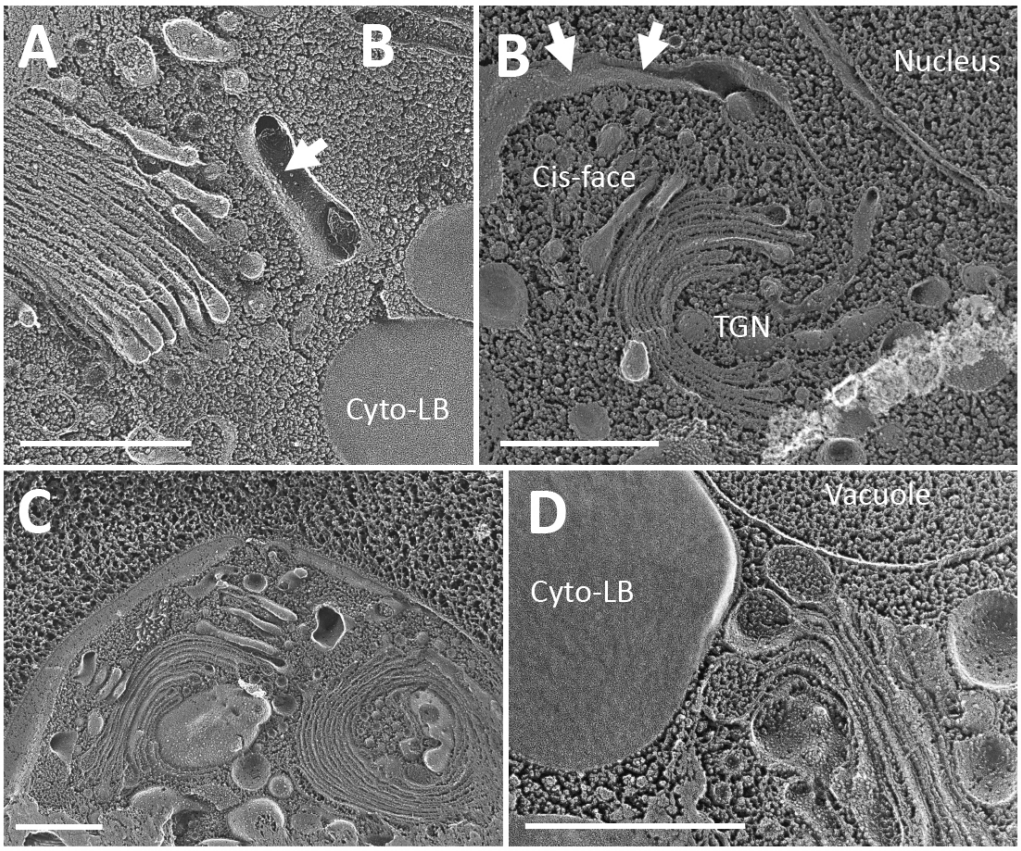

Fig. 16. Golgi apparatus. A) Cross-fracture through a stack of 11 cisternae in a green cell. Arrow: Intramembraneous particles within the endoplasmic reticulum (ER) protoplasmic-fracture face. B) Green cell Golgi stack and associated ER (arrows). Vesicles derived from the ER are joining the cis-face of the Golgi. TNG, trans-Golgi-network. C) Two contiguous Golgi stacks in an orange cell, one adopting a dome shape. D) Golgi body in an orange cell. Cyto-LB, cytoplasmic lipid body (Bars, 500nm)

3.8 Vacuoles and Autophagosomes

Vacuoles are diverse and perform multiple functions in plant and algal cells [76,77,78]. The cytoplasm of cells of *D. salina* is filled with many different kinds of round, membrane-bound vacuoles (Fig. 2, Fig.3, Fig. 17). The vacuole content may be homogeneous or include small inclusions (Fig. 17A); some were filled with crystalline substances (Fig. 17B) similar to those observed in *C. reinhardtii* (Goodenough, in preparation). Vacuoles found in some orange cells contained membrane-remnant debris (Fig. 17C, 17D) and resembled the autophagosomes of *C. reinhardtii* [79]. Possibly their formation is a response to the nutrient limitation that these cells were experiencing in late stage batch culture.

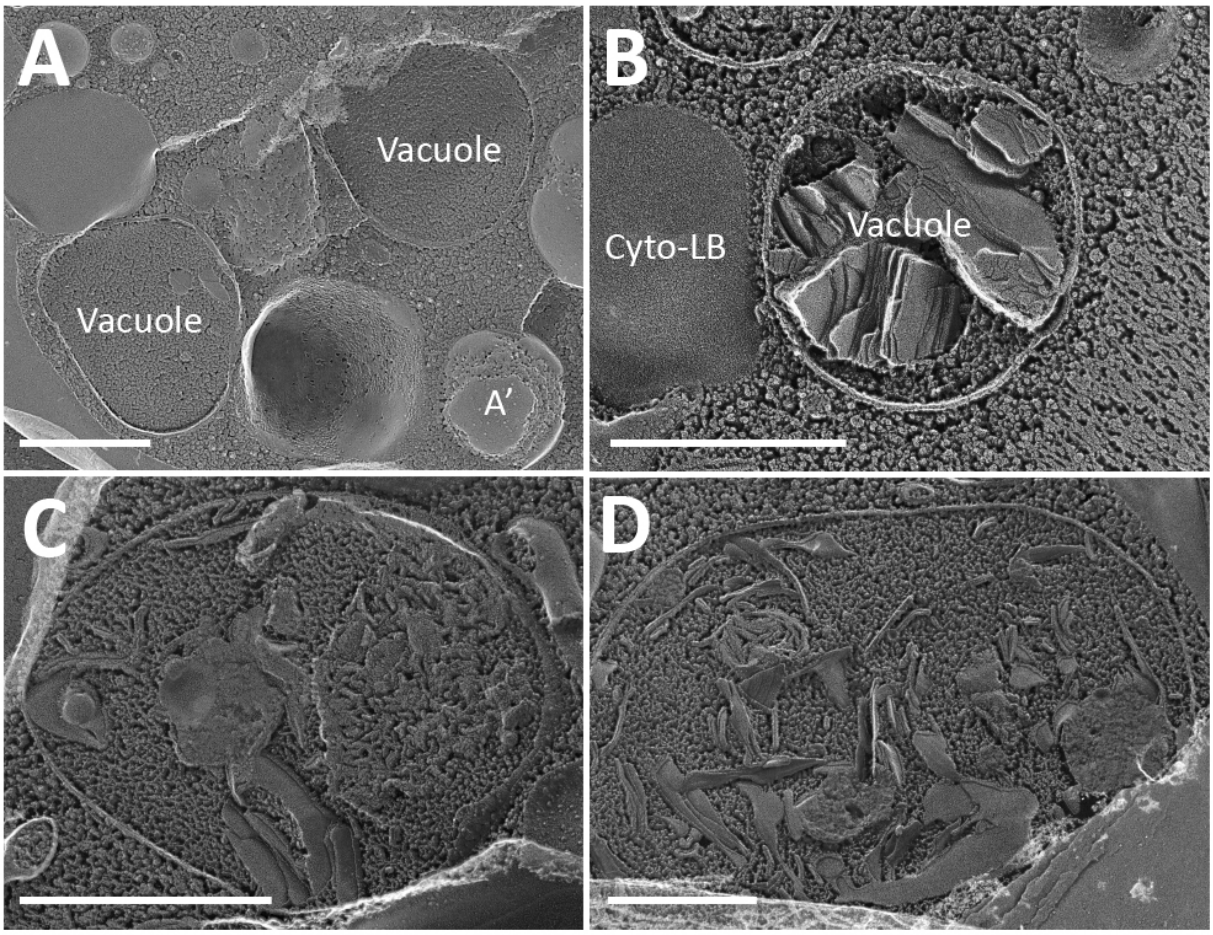

Fig. 17. Vacuoles and autophagosomes. A) Green cell with two vacuoles. B) Vacuole with crystals from a green cell. C) and D) Autophagosomes from an orange cell containing membrane-remnant debris. A', variant acidocalcisome; Cyto-LB, cytoplasmic lipid body. (Bars, 500nm)

3.9 Acidocalcisomes

Acidocalcisomes are cellular organelles with a variety of functions [89]. In *D. salina*, acidic vacuoles have been described that are involved in the storage of polyphosphate [23] and of iron [18], hallmark activities of acidocalcisomes. A recent report using QFDEEM [79] presented acidocalcisome ultrastructure in detail, primarily for *C. reinhardtii*, but with an overview of other algae and protists as well.

The acidocalcisomes of *D. salina* resemble those found in other microeukaryotes: the convex E-fracture face adopts a rugose morphology with etching (Figs. 18A and C) and the concave P-face carries a dense population of small intramembranous particles (Figs. 18B and D). Fig. 18B shows a P- and an E-fracture face side-by-side, a "twin" image also found in *C. reinhardtii* [79]. No internal polyphosphate granules were observed; it is not known whether this is due to sampling or whether granules were not assembled under the growth conditions employed [79].

In addition to these “classic” acidocalcisomes, a second organelle, which we refer to as an acidocalcisome variant (labeled A’ in Figs. 5A, 5B, 5C, and 17A) is frequently present in green cells, but has not been found in stressed orange cells nor in *Dunaliella tertiolecta*. Its E-face carries a mixture of smooth domains interspersed with IMP-rich regions (Fig. 19). We have not identified a corresponding P-face, perhaps because it is indistinguishable from a classic P face. While we designate this organelle as an acidocalcisome variant based on its similarities to classic acidocalcisomes, confirmation awaits their isolation and characterization.

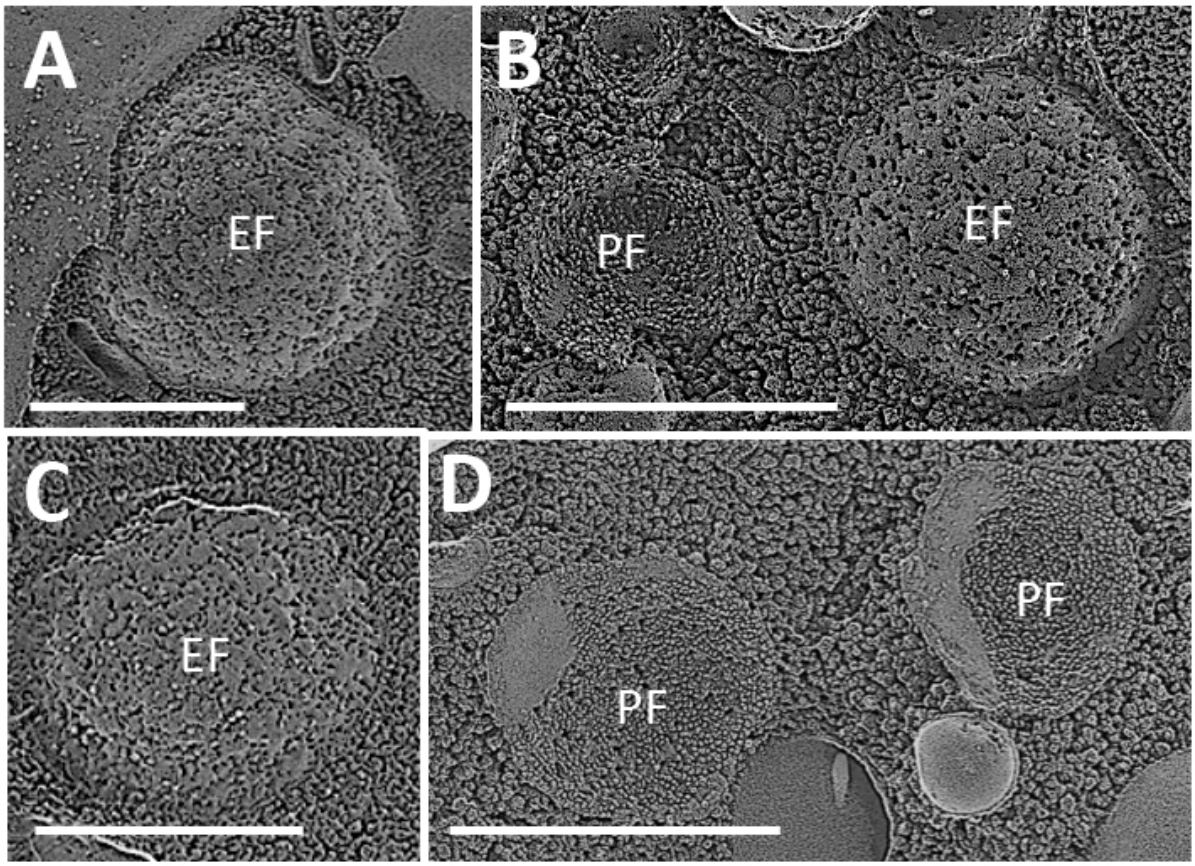

Figure 18: Acidocalcisomes. A) Exoplasmic-fracture face (EF) from an orange cell. B) EF and protoplasmic-fracture face (PF) from an orange cell. C) EF from a green cell. D) Two PFs from a green cell. (Bars, 500nm)

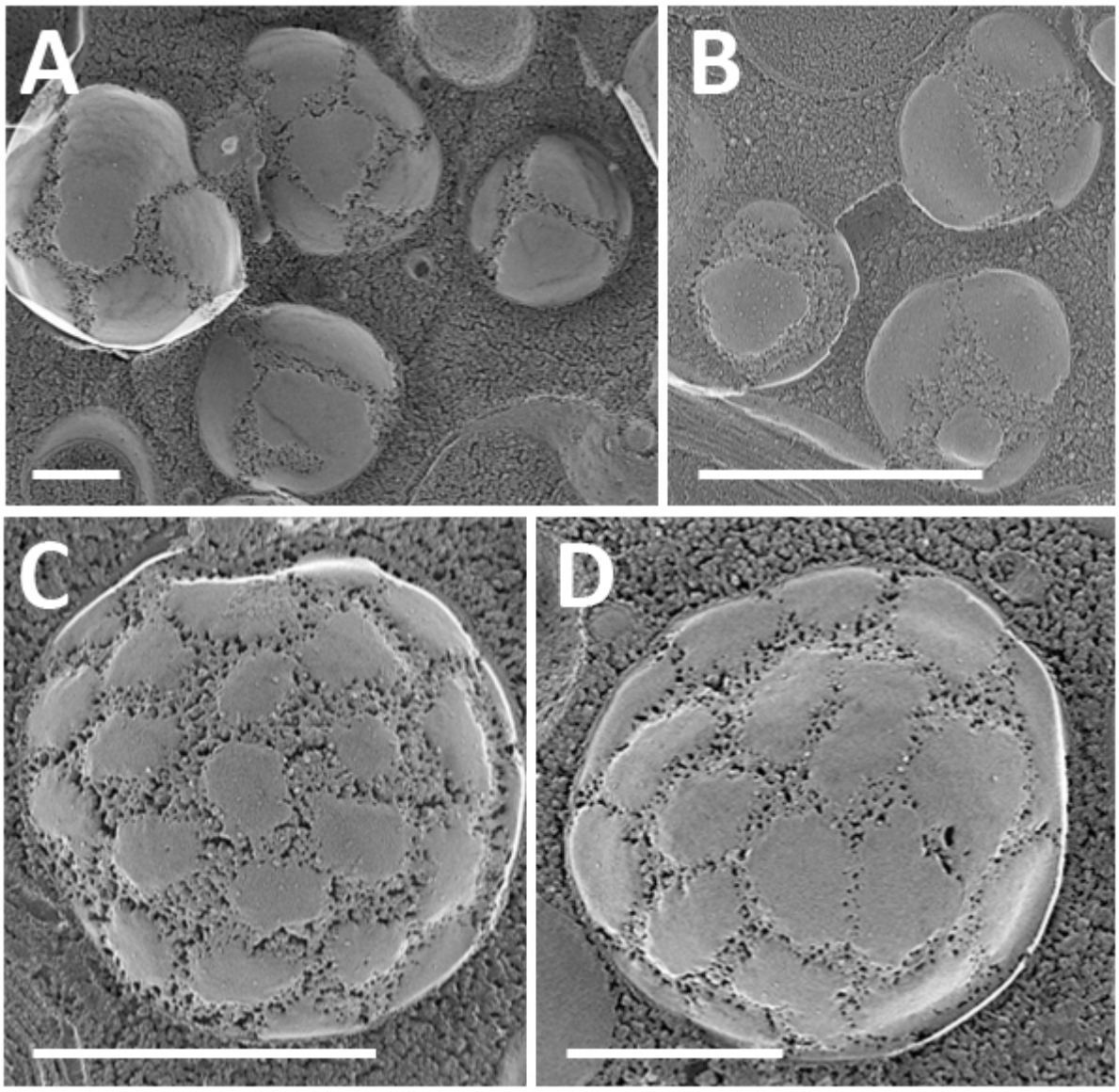

Figure 19: Exoplasmic-fracture face views of acidocalcisome variants from green cells. (Bars, 500nm)

4. Conclusions

Our findings are summarized in the schematics for a green (upper panel) and orange (lower panel) cell shown in Fig. 20. It is our hope that this in-depth understanding of *D. salina* will be of value to scientists seeking to probe the biosynthetic parameters of this important microeukaryote.

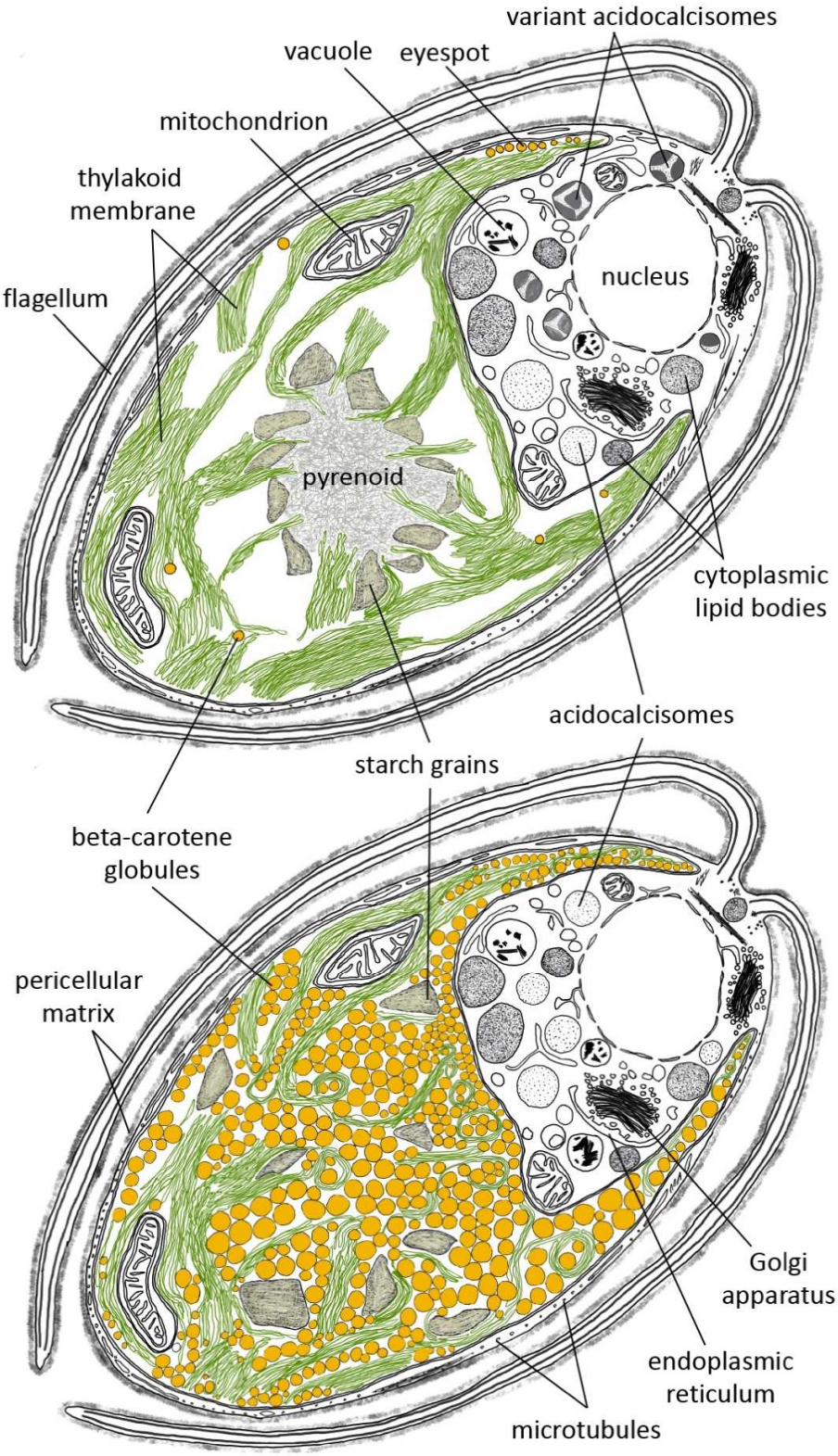

Fig. 20. The upper panel shows a green cell of *D. salina* with a chloroplast containing the thylakoid membrane arranged in appressed regions. The pyrenoid is visible in the chloroplast. The candidate

eyespot is shown in the cup of the chloroplast. In strain CCAP19/18 some single β-Carotene globules (βCGs) are dispersed throughout the chloroplast. The lower panel displays an orange cell where the chloroplast is filled with βCGs. The thylakoid membrane is reduced and in this example the starch grains do not form any pyrenoid. The pericellular matrix surrounds each of the cells, including both of the flagella.

CRediT authorship contribution statement

Juergen Polle: Conceptualization, Resources, Formal Analysis, Visualization, Writing – Original Draft. **Robyn Roth:** Investigation. **Ami Ben-Amotz:** Writing – Review & Editing. **Ursula Goodenough:** Formal analysis, Visualization, Supervision, Writing – Review & Editing.

Acknowledgements

We thank the Research Foundation of the City University of New York (JP) and the U.S. Department of Energy (UG) for funding.

Statement of informed consent

No conflicts, informed consent, human or animal rights applicable.

Declaration of author's agreement to authorship and submission

All authors have agreed to authorship and the submission of this manuscript for peer review.

Declaration of competing interest

There is no conflict of interest that could be perceived to influence the outcomes of the present research.

References

[1] Teodoresco, E.C. 1905. Organization et developpement du *Dunaliella*, nouveau genre de Volvocacee-Polyblepharidee. Beihefte Botanisches Zentralblatt, Bd.18, Abt.1, pp. 215-232.
[2] Avron M., Ben-Amotz A. (1992) *Dunaliella*: physiology, biochemistry, and biotechnology. CRC Press, Boca Raton, FL, USA. ISBN-10: 084936647X.
[3] Ben-Amotz A., Polle, J.E.W., Subba Rao D.V. (2009) The alga *Dunaliella*: biodiversity, physiology, genomics and biotechnology. Science Publishers, Enfield, NH, USA. ISBN 9781578085453.
[4] Ben-Amotz A. (1974) Osmoregulation mechanism in the halophilic alga *Dunaliella parva*. In: Membrane Transport in Plants (Eds.U. Zimmerman and J. Dainty), Springer-Verlag, Berlin-Heidelberg-New York, pp. 95-100.
[5] Ginzburg M. (1988) *Dunaliella*: A Green Alga Adapted to Salt. Advances in Botanical Research, 14 (C), pp. 93-183.

[6] Borowitzka, L.J. (1981) 4. The microflora. Adaptations to life in extremely saline lakes. Hydrobiologia, 81 (1), pp. 33–46.
[7] Massyuk N.P. (1973) Morphology, Taxonomy, Ecology and Geographic Distribution of the Genus *Dunaliella* Teod. and Prospects for its Potential Utilization. Naukova Dumka, Kiev.
[8] Preisig H.R. (1992) Morphology and taxonomy. In: *Dunaliella*: Physiology, Biochemistry, and Biotechnology. (Eds. Avron M., Ben-Amotz A.), CRC Press, Boca Raton, pp. 1–15.
[9] Borowitzka M.A., Siva C.J. (2007) The taxonomy of the genus *Dunaliella* (Chlorophyta, Dunaliellales) with emphasis on the marine and halophilic species. Journal of Applied Phycology, 19 (5), pp. 567-590.
[10] Polle J.E.W., Tran D., Ben-Amotz A. (2009) History, Distribution, and Habitats of Algae of the Genus *Dunaliella* TEODORESCO (Chlorophyceae). Chapter 1 in The alga *Dunaliella*: biodiversity, physiology, genomics and biotechnology. (Eds. Ben-Amotz A., Polle J.E.W., Subba Rao D.V.), Science Publishers, Enfield, NH, USA. ISBN 9781578085453.
[11] Xu Y., Ibrahim I.M., Wosu C.I., Ben-Amotz A., Harvey P.J. (2018) Potential of new isolates of *Dunaliella salina* for natural β-Carotene Production. Biology, 7, 14.
[12] Goodenough U., Roth R., Kariyawasam T., He A. , Lee J.-H. (2018) Epiplasts: Membrane skeletons and epiplastin proteins in Euglenids, Glaucophytes, Cryptophytes, Ciliates, Dinoflagellates, and Apicomplexans. mBio 9:e02020-18.
[13] Lee J.-H., Heuser J.E., Roth R., Goodenough U. (2015) Eisosome ultrastructure and evolution in fungi, microalgae, and lichens. Eukaryotic Cell, 14 (10), pp. 1017-1042.
[14] Weiss T.L., Roth R., Goodson C., Vitha S., Black I., Azadi P., Rusch J., (...), Goodenough U. (2012) Colony organization in the green alga *Botryococcus braunii* (Race B) is specified by a complex extracellular matrix. Eukaryotic Cell, 11 (12), pp. 1424-1440.
[15] Borowitzka, M.A. (2018a) Biology of Microalgae. Chapter 3 in Microalgae in Health and Disease Prevention. (Eds. Levine I.A., Fleurence J.), Academic Press, pp 23-72, ISBN 9780128114056.
[16] Davidi L., Shimoni E., Khozin-Goldberg I., Zamir A., Pick U. (2014) Origin of β-carotene-rich plastoglobuli in *Dunaliella bardawil*. Plant Physiology, 164 (4), pp. 2139-2156.
[17] Lamers P.P., Van De Laak C.C.W., Kaasenbrood P.S., Lorier J., Janssen M., De Vos R.C.H., Bino R.J., Wijffels R.H. (2010) Carotenoid and fatty acid metabolism in light-stressed *Dunaliella salina*. Biotechnology and Bioengineering, 106 (4), pp. 638-648.
[18] Paz Y., Shimoni E., Weiss M., Pick U. (2007) Effects of iron deficiency on iron binding and internalization into acidic vacuoles in *Dunaliella salina*. Plant Physiology, 144 (3), pp. 1407-1415.
[19] Rabbani S., Beyer P., Lintig J.V., Hugueney P., Kleinig H. (1998) Induced β-Carotene synthesis driven by triacylglycerol deposition in the unicellular alga *Dunaliella bardawil.* Plant Physiology, 116 (4), pp. 1239-1248.
[20] Katz A., Jimenez C., Pick U. (1995) Isolation and characterization of a protein associated with carotene globules in the alga *Dunaliella bardawil*. Plant Physiology, 108 (4) , pp. 1657-1664.
[21] Leonardi P.I., Caceres E.J. (1994) Comparative analysis of the fine structure of young and adult individuals of *Dunaliella salina* (Polyblepharidaceae, Chlorophyceae) with emphasis on the flagellar apparatus. Journal of Phycology, 30 (4), pp. 642-653.

[22] Giordano M., Davis J.S., Bowes G. (1994) Organic carbon release by Dunaliella salina (Chlorophyta) under different growth conditions of CO_2, nitrogen, and salinity. Journal of Phycology, 30 (2), pp. 249-257.
[23] Pick U., Weiss M. (1991) Polyphosphate hydrolysis within acidic vacuoles in response to amine-induced alkaline stress in the halotolerant alga *Dunaliella salina*. Plant Physiology, 97 (3), pp. 1234-1240.
[24] Ben-Amotz A., Lers, Avron M. (1988) Stereoisomers of β-Carotene and Phytoene in the alga *Dunaliella bardawil*. Plant Physiology, 86, pp. 1286-1291.
[25] Ben-Amotz A. and Avron M. (1987) The biotechnology of mass culturing of *Dunaliella* for products of commercial interest. Chapter 4. In: Algal and Cyanobacterial Biotechnology, pp 90-114, ISBN 9780470214770
[26] Ben-Amotz A., Avron M. (1983) On the factors which determine massive ß-carotene accumulation in the halotolerant alga *Dunaliella bardawil*. Plant Physiology, 72, pp. 593-597.
[27] Ben-Amotz A., Katz A., Avron M. (1982) Accumulation of β-Carotene in halotolerant algae: Purification and characterization of β-Carotene-rich globules from *Dunaliella bardawil*. (Chlorophyceae). Journal of Phycology, 18 (4), pp. 529-537.
[28] Ben-Amotz A., Avron M. (1981) Glycerol and ß-carotene metabolism in the halotolerant alga *Dunaliella*: a model system for biosolar energy conversion. Trends in Biochemical Sciences, 6 (C), pp. 297-299.
[29] Pfeifhofer AO, Belton JC (1975) Ultrastructural changes in chloroplasts resulting from fluctuations in NaCl concentration: freeze-fracture of thylakoid membranes in *Dunaliella salina*. Journal of Cell Science, 18, pp. 287–299.
[30] Werz G., Kellner G. (1970) The structure of the Golgi-apparatus in freeze-etched *Dunaliella* cells. Protoplasma, 69 (3-4), pp. 351-364.
[31] Trezzi F., Galli M.G., Bellini E. (1964) The ultrastructure of *Dunaliella salina*. Giornale Botanico Italiano, 71 (1-2), pp. 127-136.
[32] Ben-Amotz A. (2009) Bioactive Compounds: Glycerol production, carotenoid production, fatty acids production. Chapter 8 in in The alga *Dunaliella*: biodiversity, physiology, genomics and biotechnology. (Editors: Ben-Amotz A., Polle J.E.W., Subba Rao D.V.), Science Publishers, Enfield, NH, USA. ISBN 9781578085453.
[33] Borowitzka M.A. (2018b) The 'stress' concept in microalgal biology—homeostasis, acclimation and adaptation. Journal of Applied Phycology, 30(5), pp. 2815-2825.
[34] Borowitzka M.A., Borowitzka L.J., Kessly D. (1990) Effects of salinity increase on carotenoid accumulation in the green alga *Dunaliella salina*. Journal of Applied Phycology, 2 (2), pp. 111-119.
[35] Pick U., Zarka A., Boussiba S., Davidi L. (2019) A hypothesis about the origin of carotenoid lipid droplets in the green algae *Dunaliella* and *Haematococcus*. Planta, 249 (1), pp. 31-47.
[36] Ben-Amotz A. (1980) Glycerol, β-carotene and dry algal meal production by commercial cultivation of *Dunaliella*. (Eds. Shelef G, Soeder CJ), Algae Biomass. Amsterdam: Elsevier, pp. 603–610.
[37] Borowitzka L.J., Borowitzka M.A., Moulton T.P. (1984) The mass culture of *Dunaliella* for fine chemicals: from laboratory to pilot plant. Hydrobiologia. 1984;116/117:115–121. doi: 10.1007/BF00027649.).

[38] Borowitzka M.A. (2013) *Dunaliella*: Biology, Production, and Markets. Handbook of Microalgal Culture: Applied Phycology and Biotechnology, (Eds. Richmond A., Hu Q.), 2nd Edition, pp. 359-368.
[39] Shaish A., Ben-Amotz A., Avron M. (1991) Production and selection of high β-Carotene mutants of *Dunaliella bardawil* (Chlorophyta). Journal of Phycology, 27 (5), pp. 652-656.
[40] Polle JEW, Barry K, Cushman J, Schmutz J, Tran D, Hathwaik LT, (…), Magnuson J (2017) Draft Nuclear Genome Sequence of the Halophilic and Beta-Carotene-Accumulating Green Alga *Dunaliella salina* Strain CCAP19/18. Genome Announcements, 5(43), pii: 5/43/e01105-17.
[41] Pick U., Karni L., Avron M. (1986) Determination of ion content and ion fluxes in the halotolerant alga *Dunaliella salina*. Plant Physiology, 81, pp. 92–96.
[42] Heuser JE (2011) The origins and evolution of freeze-etch electron microscopy. Journal of Electron Microscopy, 60, S3–S29.
[43] Oliveira L., Bisalputra T., Antia N.J. (1980) Ultrastructural observation of the surface coat of *Dunaliella tertiolecta* from staining with cationic dyes and enzyme treatments. New Phytologist, 85 (3), pp. 385-392.
[44] Hatanaka Y., Inaoka K., Kobayashi O., Higashihara M., Hiyama K. (1998) Sensitivity of the surface coat of the halotolerant green alga *Dunaliella parva* (Volvocales, Chlorophyceae) to lysozyme. Phycological Research, 46 (2), pp. 147-153.
[45] Katz A., Waridel P., Shevchenko A., Pick U. (2007) Salt-induced changes in the Plasma Membrane Proteome of the Halotolerant Alga *Dunaliella salina* as revealed by blue nativ gel electrophoresis and Nano-LC-MS/MS analysis. Molecular and Cellular Proteomics, 6 (9) , pp. 1459-1472.
[46] Komaristaya V.P., Gorbulin O.S. (2006) Sporopollenin in the composition of cell walls of *Dunaliella salina* Teod. (Chlorophyta) zygotes. International Journal on Algae, 8 (1), pp. 43-52.
[47] Pick U. (1998) *Dunaliella* - A model extremophilic alga. Israel Journal of Plant Sciences, 46, pp. 131-139.
[48] Oren-Shamir M., Pick U., Avron M. (1990) Plasma membrane potential of the alga *Dunaliella*, and its relation to osmoregulation. Plant Physiology, 93 (2), pp. 403-408.
[49] Sheffer M, Fried A., Gottlieb H.E., Tietz A., Avron M. (1986) Lipid composition of the plasma-membrane of the halotolerant alga, *Dunaliella salina*. Biochimica et Biophysica Acta (BBA) – Biomembranes, 857(2), pp. 165-172.
[50] Zelazny A.M., Shaish A., Pick U. (1995) Plasma membrane sterols are essential for sensing osmotic changes in the halotolerant alga *Dunaliella*. Plant Physiology, 109 (4), pp. 1395-1403.
[51] Fisher M., Gokhman I., Pick U., Zamir A.(1996) A salt-resistant plasma membrane carbonic anhydrase is induced by salt in *Dunaliella salina*. Journal of Biological Chemistry, 271 (30), pp. 17718-17723.
[52] Katz K.R., McLean R.J. (1979) Rhizoplast and rootlet system of the flagellar apparatus of *Chlamydomonas moewusii*. Journal of Cell Science, 39, pp. 373-381.
[53] Engel B.D., Schaffer M., Cuellar L.K., Villa E., Plitzko J.M., Baumeister W. (2015) Native architecture of the *Chlamydomonas* chloroplast revealed by in situ cryo-electron tomography. eLife, 2015 (4), art. no. e04889.

[54] Loeblich L.A. (1982) Photosynthesis and Pigments Influenced By Light Intensity and Salinity in the Halophile *Dunaliella salina* (Chlorophyta). Journal of the Marine Biological Association of the United Kingdom, 62 (3), pp. 493-508.
[55] Rottet S., Besagni C., Kessler F. (2015) The role of plastoglobules in thylakoid lipid remodeling during plant development. Biochimica et Biophysica Acta - Bioenergetics, 1847 (9), art. no. 47424, pp. 889-899.
[56] Griffiths D.J. (1980) The pyrenoid and its role in algal metabolism. Science Progress, 66 (264), pp. 537-553.
[57] Kreimer G. (2009) The green algal eyespot apparatus: A primordial visual system and more? Current Genetics, 55 (1), pp. 19-43.
[58] Shenoy, Preetha & John, Lijo & C S, Subin & KK, Vijayan. (2012). Phenotypic and genetic characterization of *Dunaliella* (Chlorophyta) from Indian salinas and their diversity. Aquatic Biosystems. 8. 27. 10.1186/2046-9063-8-27.
[59] Goodson C., Roth R., Wang Z.T., Goodenough U. (2011) Structural correlates of cytoplasmic and chloroplast lipid body synthesis in *Chlamydomonas reinhardtii* and stimulation of lipid body production with acetate boost. Eukaryotic Cell, 10 (12), pp. 1592-1606.
[60] Posudin Y., Massjuk N., Lilitskaya G. (2010) Photomovement of *Dunaliella* Teod. 1st Edition, Publisher: Vieweg and Teubner Verlag, Germany. DO - 10.1007/978-3-8348-9765-7
[61] Zhang F., Vierock J., Yizhar O., Fenno L.E., Tsunoda S., Kianianmomeni A., (...), Deisseroth K. (2011) The microbial opsin family of optogenetic tools. Cell, 147 (7), pp. 1446-1457.
[62] Davidi L., Levin Y., Ben-Dor S., Pick U. (2015) Proteome analysis of cytoplasmatic and plastidic β-carotene lipid droplets in *Dunaliella bardawil*. Plant Physiology, 167 (1), pp. 60-79.
[63] Lichtenthaler H.K., Sprey B. (1966) Über die osmiophilen globulären Lipideinschlüsse der Chloroplasten. Zeitschrift fur Naturforschung - Section B Journal of Chemical Sciences, 21 (7), pp. 690-697.
[64] van Wijk K.J. and Kessler F. (2017) Plastoglobuli: Plastid microcompartments with integrated functions in metabolism, plastid developmental transitions, and environmental adaptation. Annual Review of Plant Biology, 68 (1), pp. 253 -289.
[65] Austin II J.R., Frost E., Vidi P.-A., Kessler F., Staehelin L.A. (2006) Plastoglobules are lipoprotein subcompartments of the chloroplast that are permanently coupled to thylakoid membranes and contain biosynthetic enzymes. Plant Cell, 18 (7), pp. 1693-1703.
[66] Kirchhoff H. (2019) Chloroplast ultrastructure in plants. New Phytologist, 223 (2), pp. 565-574.
[67] Zienkiewicz K., Du Z.-Y., Ma W., Vollheyde K., Benning C. (2016) Stress-induced neutral lipid biosynthesis in microalgae — Molecular, cellular and physiological insights. Biochimica et Biophysica Acta - Molecular and Cell Biology of Lipids, 1861 (9), pp. 1269-1281.
[68] Li-Beisson Y., Thelen J.J., Fedosejevs E., Harwood J.L. (2019) The lipid biochemistry of eukaryotic algae. Progress in Lipid Research, 74, pp. 31-68.
[69] Davidi L., Katz A., Pick U. (2012) Characterization of major lipid droplet proteins from *Dunaliella*. Planta, 236 (1), pp. 19-33.
[70] McKie-Krisberg Z.M., Laurens L.M.L., Huang A., Polle J.E.W. (2018) Comparative energetics of carbon storage molecules in green algae. Algal Research, 31, pp. 326-333.

[71] Bonnefond H., Moelants N., Talec A., Mayzaud P., Bernard O., Sciandra A. (2017) Coupling and uncoupling of triglyceride and beta-carotene production by *Dunaliella salina* under nitrogen limitation and starvation. Biotechnology for Biofuels, 10 (1), art. no. 25.
[72] Hu Q., Sommerfeld M., Jarvis E., Ghirardi M., Posewitz M., Seibert M., Darzins A. (2008) Microalgal triacylglycerols as feedstocks for biofuel production: Perspectives and advances. Plant Journal, 54 (4), pp. 621-639.
[73] Takeuchi, T., Benning, C. (2019) Nitrogen-dependent coordination of cell cycle, quiescence and TAG accumulation in *Chlamydomonas*. Biotechnology for Biofuels, 12(1), 292.
[74] van de Meene A.M.L., Doblin M.S., Bacic A. (2017) The plant secretory pathway seen through the lens of the cell wall. Protoplasma, 254 (1), pp. 75-94.
[75] Kang B.-H., Staehelin L.A. (2008) ER-to-Golgi transport by COPII vesicles in *Arabidopsis* involves a ribosome-excluding scaffold that is transferred with the vesicles to the Golgi matrix. Protoplasma, 234 (1-4), pp. 51-64.
[76] Marty F. (1999) Plant vacuoles. Plant Cell, 11 (4) , pp. 587-599.
[77] Becker B. (2007) Function and evolution of the vacuolar compartment in green algae and land plants (Viridiplantae). International Review of Cytology, 264, pp. 1-24.
[78] Tan X., Li K., Wang Z., Zhu K., Tan X., Cao J. (2019) A review of plant vacuoles: Formation, located proteins, and functions. Plants, 8 (9), art. no. 327.
[79] Goodenough U., Heiss A.A., Roth R., Rusch J., Lee J.-H. (2019) Acidocalcisomes: Ultrastructure, Biogenesis, and Distribution in Microbial Eukaryotes. Protist, 170 (3), pp. 287-313.
[80] Docampo R., Huang G. (2016) Acidocalcisomes of eukaryotes. Current Opinion in Cell Biology, 41, pp. 66-72.